CXCL9, granzyme B and TNF-α orchestrate protective *in vitro* granulomatous responses across *Mycobacterium tuberculosis* complex lineages

Ainhoa Arbués[1,2,#], Sarah Schmidiger[1,2], Miriam Reinhard[1,2], Sònia Borrell[1,2], Sébastien Gagneux[1,2], Damien Portevin[1,2,*]

[1] Swiss Tropical and Public Health Institute, Allschwil, Switzerland.

[2] University of Basel, Basel, Switzerland.

[#] Current address: Departamento de Microbiología, Pediatría, Radiología y Salud Pública, Facultad de Medicina, Universidad de Zaragoza, Zaragoza, Spain.

[*] Corresponding author: damien.portevin@swisstph.ch

ABSTRACT

The members of the *Mycobacterium tuberculosis* complex (MTBC) causing human tuberculosis comprise ten phylogenetic lineages that differ in their geographical distribution. The human consequences of this phylogenetic diversity remain poorly understood. Here, we assessed the phenotypic properties at the host-pathogen interface of 14 clinical strains representing five major MTBC lineages. Using a human *in vitro* granuloma model combined with bacterial load assessment, microscopy, flow cytometry, and multiplexed-bead arrays, we observed considerable intra-lineage diversity. Yet, modern lineages were overall associated with increased growth rate and more pronounced granulomatous responses. MTBC lineages exhibited distinct propensities to accumulate triglyceride lipid droplets —a phenotype associated with dormancy— that was particularly pronounced in lineage 2 and reduced in lineage 3 strains. The most favorable granuloma responses were associated with strong CD4 and CD8 T cell activation as well as inflammatory responses mediated by CXCL9, granzyme B and TNF-α. Both of which showed consistent negative correlation with bacterial proliferation across genetically distant MTBC strains of different lineages. Taken together, our data indicate that different virulence strategies and protective immune traits associate with MTBC genetic diversity at lineage and strain level.

INTRODUCTION

With an estimated 1.3 million deaths in 2022, tuberculosis (TB) remains one of the deadliest

33 infectious diseases in the world (WHO, 2023). The main etiological agents of TB are a group of closely
34 related bacteria collectively known as the *Mycobacterium tuberculosis* complex (MTBC). Human-
35 adapted MTBC strains are classified into ten phylogenetic lineages (L1 to L10), which are considered
36 "ancestral" (L1 and L5 to L10) or "modern" (L2 to L4) based on the presence or absence of the TbD1
37 genomic region (Brosch et al., 2002; Comas et al., 2013; Coscolla et al., 2021; Guyeux et al., 2024).
38 Among these lineages, L1 to L4 are responsible for most of the TB cases worldwide; with less
39 prevalent lineages restricted to specific African regions. Local adaptation to specific human hosts
40 has been proposed to support this uneven phylogeographic distribution and disease burden of
41 different MTBC lineages (Gagneux et al., 2006). Irrespective of the underlying reason for this
42 phylogeographic population structure, the clinical implications of MTBC genetic diversity,
43 particularly on vaccine efficacy, remains unclear (Perez et al., 2020).
44 Clinical and epidemiological studies have suggested that MTBC strains might contribute differently
45 to disease presentation and transmissibility; with the difference between ancestral and modern
46 lineages being particularly marked. For example, several reports have described an association
47 between ancestral L1 and higher rates of extrapulmonary TB (Caws et al., 2008; Click et al., 2012;
48 Saelens et al., 2022; Seraphin et al., 2017). Moreover, strains belonging to ancestral lineages display
49 a lower capacity to transmit compared to strains from the modern lineages L2 and L4 (Caws et al.,
50 2008; Guerra-Assuncao et al., 2015; Nebenzahl-Guimaraes et al., 2015). However, these measures
51 of virulence are influenced by non-bacterial factors, such as host genetics and immune competency
52 or delays in health care seeking or access. The first experimental clues regarding the phenotypic
53 consequences of strain genetic variation in the MTBC date from the 1960s with the observation that
54 South Indian isolates were less virulent than strains from British patients in the guinea pig model
55 (Mitchison et al., 1960). Since then, much of our knowledge on the implications of MTBC diversity
56 came from studies characterizing outbreak-causing strains (Manca et al., 1999; Manca et al., 2001;
57 Newton et al., 2006), or focusing on only a few representative strains of specific lineages (Hiza et al.,
58 2023; Romagnoli et al., 2018). However, extrapolation of strain-specific characteristics to an entire
59 lineage can be misleading due to considerable intra-lineage heterogeneity in experimental outcomes
60 (Portevin et al., 2011; Reiling et al., 2013; Wang et al., 2010). Furthermore, even though awareness
61 of strain variation and its consequences is raising, the majority of immunological studies are based
62 on laboratory-adapted reference strains such as H37Rv or Erdman. In addition, our understanding of
63 immune protective traits in TB remains insufficient and yet dominated by data from mouse and non-
64 human primate studies (Esaulova et al., 2021; Gideon et al., 2022; Moreira-Teixeira et al., 2020;
65 Plumlee et al., 2021).

66 We previously demonstrated the clinical relevance of a three-dimensional (3D) *in vitro* granuloma
67 model —which encompasses, with the exception of neutrophils, all immune cell types involved in
68 TB— by mechanistically dissecting the differential resuscitation of MTB in granulomas exposed to
69 distinct TNF-α antagonists (Arbues et al., 2020a). In this study, we aimed to extend this *in vitro*
70 granuloma model to the study of a large collection of well-characterized and genetically diverse
71 representatives of the MTBC (Borrell et al., 2019). We assessed bacterial virulence in terms of growth
72 rate and characterized the individual immune responses to the various MTBC strains. Our results
73 reveal a broad spectrum of granulomatous responses that correlate with the level of mycobacterial
74 proliferation. Overall, strains of the modern lineages are associated with higher growth rates that
75 correlate with increased macrophage cell death and granuloma scores (based on size and shape);
76 nevertheless, we also report substantial intra-lineage heterogeneity. Furthermore, our results show
77 that granulomatous responses associated with the least replicating strains harbor an increased CD4
78 and CD8 T cell activation as well as the release of specific soluble factors encompassing CXCL9,
79 granzyme B and TNF-α.
80
81 **RESULTS**
82 **Mycobacterial growth in human *in vitro* granulomas shows marked intra-lineage diversity and is**
83 **overall increased for MTBC modern lineages**
84 We selected 14 isolates (Table 1) from a reference set of clinical strains covering much of the global
85 diversity of the human-adapted MTBC (Borrell et al., 2019). As a first measure of virulence, we
86 evaluated the capacity of the strains to proliferate within 3D *in vitro* granulomas. Bacterial load
87 based on colony forming units (CFU) was quantified on days one and eight post-infection (p.i.) to
88 determine the growth rate between these time points. The different strains proliferated with rates
89 ranging from 8.1 to 136.0 (Figure 1). Modern lineages (L2 to L4) proliferated significantly more than
90 ancestral ones (L1 and L5) did (median rates 52.1 [modern] vs. 27.2 [ancestral], $p < 0.001$ by Mann-
91 Whitney test) (Figure 1A). Stratification of the data by lineage revealed that the growth rate of L2
92 tended to be higher than that of the other modern lineages (median rates 76.0 [L2] vs. 45.1 [L3] and
93 53.7 [L4]) (Figure 1B). Nevertheless, substantial intra-lineage heterogeneity could be observed,
94 particularly within L1 and L2 (Figure 1C). The lower virulence observed for ancestral lineages in
95 general was contrasted by strain L1B that displayed a high growth rate (median 64.7) comparable to
96 that of most strains belonging to modern lineages. Moreover, while L2 Beijing strains (L2B and L2C)
97 exhibited a characteristic hyper-virulent phenotype (median rates 76.0 and 111.6, respectively), the
98 proto-Beijing L2A was one of the most attenuated strains (median 14.7). In comparison, L3 to L5

representative strains behaved more homogeneously. Noteworthy, the reference strain H37Rv, belonging to L4, displayed a lower growth rate than any of the evaluated L4 clinical isolates. Taken together, our results confirm the higher virulence propensities of strains from modern lineages, and L2 Beijing strains in particular, although they also highlight considerable intra-lineage diversity.

Propensity to enter dormancy is particularly pronounced in lineage 2 and reduced in lineage 3 strains

MTBC pathogenicity relies on its ability to survive the hostile and hypoxic granulomatous environment. The transcription factor DosR orchestrates the adaptation to oxygen limitation by inducing a metabolic switch into a dormant state (Garton et al., 2008; Gengenbacher and Kaufmann, 2012). A constitutive over-expression of *dosR* in L2 Beijing strains has been proposed to contribute to their enhanced virulence and transmissibility (Reed et al., 2007). A genomic duplication including the DosR operon and a synonymous SNP within Rv3134c, which generates an alternative transcriptional start site, have been linked to this increased expression of the DosR regulon (Domenech et al., 2010; Domenech et al., 2017). A hallmark of our *in vitro* granuloma model resides in the generation of a hypoxic environment leading to dormant-like MTBC features such as the loss of acid-fastness and accumulation of triacylglycerides, which can be quantified by differential auramine-O (Au)/Nile red (NR) fluorescent staining (Arbues et al., 2020a; Arbues et al., 2021). We assessed whether MTBC genetic diversity would result in a differential propensity to enter dormancy when facing a hypoxic environment. Therefore, we quantified the ratio between dormant (Au^{-} NR^{+}) and metabolically active (Au^{+} NR^{-}) bacteria (hereafter referred to as 'dormancy ratio') for each MTBC strain (Figure 2A). While approximately 50% of H37Rv bacilli acquired dormant-like features (median dormancy ratio 0.94), other MTBC clinical strains showed a level of dormancy induction spanning from 0.29 to 1.98. Upon grouping strains by lineage (Figure 2B), no significant difference was found between L1, L4 and L5 (median dormancy ratios 0.85 [L1], 0.86 [L4], and 1.06 [L5]). Nonetheless, L2 strains exhibited an increased propensity to accumulate triacylglycerides (median dormancy ratio 1.30; $p = 0.072$ vs. L1 and $p < 0.05$ vs. L4 by corrected Dunn's multiple comparisons test). This result is in line with the fact that they are carriers of the aforementioned genomic events: the duplication in L2A, the Rv3134c SNP in L2B, and both in L2B. By contrast, L3 bacilli seemed more prone to remain in a metabolically active state in comparison to bacteria belonging to the other lineages (median dormancy ratio 0.54; $p = 0.072$ vs. L5 by corrected Dunn's multiple comparisons test). Interestingly, the ratio between dormant and metabolically active bacilli showed no correlation with the respective growth rate of the individual MTBC strains (Figure 2C). This finding suggests that an increased ability to enter dormancy is not necessarily associated with a more pronounced growth

132 phenotype. Further studies are necessary to better understand the dormancy ratio-growth rate
133 relationship, and to assess how this might relate to *in vivo* virulence.

134 **MTBC strain diversity translates into a spectrum of granulomatous responses that correlates with**
135 **bacterial growth and induction of macrophage apoptosis**

136 We next investigated the impact of MTBC strain diversity on the host immune responses within *in*
137 *vitro* granulomas. We monitored cellular aggregation by bright field microscopy imaging on day 7
138 p.i., and quantified the area and aspect ratio of the individual aggregates as well as their total
139 number. While uninfected (UI) PBMCs did not lead to significant aggregation, all MTBC strains
140 induced the formation of *in vitro* granulomas in variable numbers, shapes and sizes (Figure 3A).
141 Despite notable donor-to-donor variability, the differential granulomatous responses induced by the
142 individual strains were consistent across all donors (Supplementary figure 1). Overall, 10 to 58 *in*
143 *vitro* granulomas were identified per field (Supplementary figure 2A). Strains L1A, L2A and L5B
144 displayed a tendency to induce more aggregates per field (median 42.5 [L1A], 40 [L2A] and 31.5
145 [L5B] vs. 22 [across all strains]) that were characterized by a less circular shape (i.e., higher aspect
146 ratio) (median aspect ratios 1.38 [L1A], 1.35 [L2A] and 1.33 [L5B] vs. 1.25 [across all strains])
147 (Supplementary figure 2B). By contrast, L3 and L4 strains triggered the formation of markedly larger
148 granulomas (median average area per granuloma in μm^2: 6,586.4 [L3] and 7,800 [L4] vs. 3,377.8 [L1],
149 5,199.2 [L2] and 4,638.4 [L5]) (Supplementary figure 2C). In order to simplify the ensuing analyses,
150 we integrated these parameters into a granuloma score (see Methods) that reflects the gamut of
151 responses observed so that the bigger and more circular the granulomas, the higher the granuloma
152 score (Figure 3B). Granuloma scores ranged from 42.2 to 1,801.1, with a median of 199.5. Infection
153 with modern lineages, especially L3 and L4, led to granulomatous responses with significantly higher
154 scores (median granuloma scores 205.6 [L2], 374.8 [L3] and 290.2 [L4] vs. 107.2 [L1] and 130.2 [L5])
155 (Figure 3C). Interestingly, the granuloma score showed a significant positive correlation with the
156 respective strain growth rate (Figure 3D).

157 It has been reported that apoptosis of infected macrophages drives early dissemination and
158 granuloma formation (Aguilo et al., 2013; Davis and Ramakrishnan, 2009). Therefore, we sought to
159 evaluate macrophage apoptosis induced by the various strains in the context of granulomatous
160 responses using flow cytometry (Supplementary figure 3). We did not observe significant differences
161 in the total number of $CD11b^+$ macrophages recovered six days after infection with the various MTBC
162 strains. Overall, the percentage of apoptotic macrophages (annexin V^+ 7-AAD^-) ranged from 24.3%
163 to 65.2%, with a median of 41.2% (Figure 4A). Most of the strains shared intermediate levels of
164 macrophage apoptosis, including the reference strain H37Rv (median percentage of apoptotic

165 macrophages 40.2%). By contrast, L1A and L2A strains, which were associated with the lowest
166 growth rates and granulomatous responses, also exhibited a reduced induction of macrophage
167 apoptosis (median percentages 29.6% and 30.2%, respectively); whilst L2C, the most virulent strain,
168 induced the highest apoptosis levels (median percentage of apoptotic macrophages 49.4%). In fact,
169 the percentage of apoptotic macrophages showed a significant positive correlation with the
170 replication rate of the respective infecting MTBC strain (Figure 4B) as well as with granuloma scores
171 (Figure 4C). Taken together, our results suggest that strains exhibiting greater proliferation are more
172 prone to induce macrophage apoptosis, thereby contributing to the extent of the granulomatous
173 response.

174 **Rapid lymphocyte activation as well as CXCL9, granzyme B and TNF-α secretion are associated**
175 **with reduced mycobacterial growth across the MTBC**

176 We next sought to profile the immune granulomatous responses induced the MTBC strains and
177 relate them to their respective growth rate. We first monitored by flow cytometry lymphocyte
178 proliferation using carboxyfluorescein succinimidyl ester (CFSE) dilution assay, as well as lymphocyte
179 activation based on the expression of surface markers CD69, CD25, HLA-DR and CD38 on day 6 p.i.
180 by flow cytometry (Supplementary figure 4). We focused our analysis on CD69-, CD38-, CD25- and
181 HLA-DR-expressing CD4 T cells, along with CD69- and CD38-expressing CD8 T cells, whose frequency
182 increased consistently across all donors upon infection with at least one strain (compared to the
183 uninfected control) (Supplementary figure 5). To account for inter-donor variability, we scaled the
184 responses of every donor dividing the individual response to each strain by the average response
185 across all strains of that same donor (Figure 5A). As depicted in Figure 5B, granulomatous responses
186 elicited by L1A, L2A and both L5 strains entailed marked CD4 T cell proliferation. Across all MTBC
187 strains, proliferation was consistently associated with an increased expression of the assessed
188 activation markers on both CD4 and CD8 T cells. Nevertheless, most activated CD4 T cells expressed
189 only one of the studied markers (Figure 5C). Overall, ancestral lineages were the most potent
190 inducers of all the aforementioned T cell populations (Figure 5D and Supplementary figure 6A), with
191 CD38-expressing CD4 T cells constituting the most differentially induced population (median scaled
192 frequencies 1.21 [ancestral] vs. 0.79 [modern]). Among modern lineages, L4 induced the strongest
193 T cell activation (Figure 5E and Supplementary figure 6B), which actually was not statistically
194 different from that elicited by ancestral strains (Figure 5D and Supplementary figure 6A). Infection
195 with L4 strains resulted in significantly higher percentages of CD38-positive CD4 T cells compared to
196 L2 Beijing strains (median scaled frequencies 0.94 vs. 0.54, respectively), while L3 strains elicited
197 intermediate responses (median scaled frequency 0.73). When considering bacterial growth, strains

198 eliciting an enhanced T cell response appeared among the ones replicating the least. We computed
199 Spearman's rank correlation tests with Benjamin-Hochberg multiple testing correction between CD4
200 and CD8 T cell responses and the growth rate (Figure 5F and Supplementary figure 6C). CD4 T cell
201 proliferation as well as all expression of all activation markers exhibited significant, moderate to
202 strong, negative correlations with MTBC strain growth rate, with the expression of CD38 resulting in
203 the strongest coefficient. Activation of CD8 T cells, determined by the expression of either CD38 or
204 CD69, was also significantly associated with a hampered mycobacterial proliferation. Taken together,
205 our data indicate that stronger T cell activation is associated with MTBC isolates exhibiting low
206 bacterial replication, irrespective of the lineage they belong to.
207 Subsequently, we investigated whether a panel of soluble immune factors —linked or not to T cell
208 activation— may also be associated with a reduced bacterial growth. We focused our analysis on
209 molecules present in granuloma supernatants on days 1 or 8 p.i. that were modulated by the
210 infection (Supplementary figure 7). We again scaled the data to account for inter-donor variability,
211 as described above (Figure 6A). Differentially modulated molecules included the innate cytokines
212 TNF-α and IL-1β at both time points, IL-10 and the chemokine CXCL9 at the earlier time point, and
213 IFN-γ, IL-17 (A and F), IL-22, IL-13 and granzyme B at the later (Figure 6B). Among these, IL-1β and
214 IL-13 displayed significant lineage-associated trends. L4, and to a lesser extent L3, induced a
215 significantly higher secretion of IL-1β on day 1 p.i. (median scaled responses 1.54 [L4] and 1.31 [L3]
216 vs. 0.55 [L1], 0.94 [L2], and 0.89 [L5]) (Figure 6C, *left*). This pattern remained at the later time point
217 for L4 (median scaled responses 1.37 [L4] vs. 0.79 [L1], 0.95 [L2], 1.17 [L3] and 1.03 [L5]) (Fig 6B,
218 *right*). Interestingly, the IL-1β response on day 1 p.i. showed a moderate positive correlation with
219 granuloma score (Figure 6D). Moreover, we found that the CD4 T helper 2 cytokine IL-13 was
220 preferentially induced in the context of infection with modern lineages compared to ancestral
221 lineages (median scaled responses 1.18 [modern] vs. 0.78 [ancestral]) (Figure 6E). Hence, IL-13
222 secretion exhibited a weak, but significant, positive correlation with the growth rate of the MTBC
223 strains in granulomas (Figure 6F and Supplementary figure 8). While we found no significant
224 correlation for IFN-γ, induction of CXCL9 secretion on day 1 p.i., and granzyme B as well as TNF-α on
225 day 8 p.i. were associated with a reduced MTBC bacterial proliferation. Altogether, these results
226 convey that a robust T cell activation characterized by an early CXCL9 detection and higher levels of
227 TNF-α and granzyme B may orchestrate the control of mycobacterial growth.
228
229 **DISCUSSION**
230 There is increasing epidemiological and experimental evidence that MTBC strain diversity may

231 influence pathogenicity. Yet, only a small number of studies based on human specimens have
232 compared a diverse range of strains belonging to more than two lineages (Portevin et al., 2011;
233 Reiling et al., 2013). Here, we combine an *in vitro* granuloma model (Arbues et al., 2020a; Arbues et
234 al., 2021) with a set of representative L1 to L5 strains (Borrell et al., 2019) to demonstrate that MTBC
235 genetic variation affects the crosstalk with human immune cells. We show that MTBC isolates display
236 a range of growth rates correlating with the induction of macrophage apoptosis and the extent of
237 the resulting granulomatous structures. This result is in agreement with the current view of the
238 tuberculous granuloma as a structure that, beyond functioning as purely host-protective, is exploited
239 by pathogenic mycobacteria as a niche for proliferation and dissemination (Pagan and
240 Ramakrishnan, 2014). Our data reveal various features that associate with certain MTBC lineages
241 and/or strains. Noteworthy, we have identified immune response traits that correlate with
242 hampered mycobacterial proliferation.
243 "Modern" lineages (L2 to L4) are often associated with globally spread TB epidemics, whereas TbD1-
244 intact "ancestral" lineages (L1 and L5 to L10) rather represent endemic strains restricted to a given
245 geographical area. A general consensus arose that strains belonging to modern lineages would
246 exhibit enhanced capacities to proliferate compared to those from ancestral ones (Reiling et al.,
247 2013; Romagnoli et al., 2018). Actually, in an elegant work using recombinant strains, Bottai and
248 colleagues demonstrated that TbD1 deletion significantly increases MTB virulence in relevant
249 infection models (Bottai et al., 2020). In line with these previous studies, ancestral lineages display
250 reduced virulence in *in vitro* granulomas compared to the modern lineages. L1 is found in countries
251 along the rim of the Indian Ocean. This geographical confinement together with experimental
252 evidence (Bottai et al., 2020; Reiling et al., 2013; Romagnoli et al., 2018) prompted a general view
253 of L1 as a low virulence lineage. Our data showed that, overall, L1 exhibited lower virulence than
254 modern lineages. Nonetheless, we observed a significant intra-lineage variation, with strain L1C
255 exhibiting a growth rate comparable to those of strains belonging to modern lineages. This
256 phenotypic variability may be a reflection of the highly diverse population structure exhibited by this
257 lineage (Netikul et al., 2021). In line with our findings, Mitchison and colleagues also documented a
258 wide range of virulence among South Indian isolates, with one-third of them being as virulent as the
259 British ones (Mitchison et al., 1960). Even though it is unclear whether all those strains belonged to
260 L1, we can assume that a majority of them were when considering epidemiological data (Poonawala
261 et al., 2020). These results exposing virulence variation across L1 isolates challenge the "low
262 virulence" attribute generally given to L1. However, a recent report revealed that the contribution
263 of L1 to the global TB pandemic is generally undervalued (Netikul et al., 2021). Due to its prevalence

264 in countries with the highest TB incidence, L1 was estimated to account for 28% of the total TB cases.
265 Interestingly, the strains with the higher replication rates, L1B and L1C, were isolated from patients
266 of Indian and Filipino origin and belong to the most common sublineages, L1.1.2 and L1.2.1,
267 respectively. Taken together these data suggest that some L1 sublineages may have evolved
268 mechanisms to compensate for the attenuation associated to the presence of TbD1 (Bottai et al.,
269 2020). Meanwhile, L5, previously known as *M. africanum* 1, is geographically restricted to West
270 Africa. Experimental data on L5 are scarce and most of our understanding about TB caused by *M.*
271 *africanum* derives from the study of L6, previously reported as *M. africanum* 2 (Silva et al., 2022). In
272 contrast to the down-regulation of the DosR regulon reported in the sputum of L6-infected patients
273 compared to L4 (Ofori-Anyinam et al., 2017), we observed a similar induction of dormant-like
274 mycobacteria in L4 and L5. In accordance with their ancestral genotype, both L5 strains displayed
275 comparable low replication rates and elicited increased frequencies of activated T cells.
276 Nevertheless, we cannot dismiss a potential contribution of host genetics to the apparent
277 attenuation of L5. In Ghana, infection by L5 has been associated with the Ewe ethnic group (Asante-
278 Poku et al., 2015). L5 strains displayed lower growth in macrophages from the Akan ethnic group;
279 still, proliferation in Ewe's macrophages was comparable to that of L4 isolates (Osei-Wusu et al.,
280 2023).
281 The three modern lineages (L2 to L4) displayed comparable growth rates overall. Again, substantial
282 strain-to-strain variability was observed within L2. The L2 Proto-Beijing strain L2A was markedly
283 attenuated to a level comparable to that of the ancestral lineages. At the other end of the virulence
284 spectrum, the representative of the most recently evolved L2 strains, the so-called "modern" L2
285 Beijing, displayed the highest proliferative capacity across all the MTBC strains studied. For its part,
286 the "ancestral" Beijing isolate exhibited a bacterial burden comparable to those of strains belonging
287 to other modern lineages. This finding suggests that L2 strains have evolved towards increased
288 virulence. This is also consistent with prior studies showing that modern Beijing strains exhibited
289 enhanced virulence in mice compared to those with an ancestral genotype (Ribeiro et al., 2014). The
290 L2 Beijing sublineage has received particular attention due to its high transmissibility and virulence
291 in cellular and animal models (Guerra-Assuncao et al., 2015; Manca et al., 2001; Tram et al., 2018;
292 Tsenova et al., 2005). One previously identified mechanism contributing to the hyper-virulent
293 phenotype of L2 Beijing strains is the inhibition of the production of pro-inflammatory cytokines
294 (Reed et al., 2004; Wang et al., 2010). Likewise, we found that both L2 Beijing strains were poor
295 inducers of T cell activation and pro-inflammatory cytokines. By contrast, we found the high
296 replication rate of L4 strains to be accompanied by a significant T cell activation and high levels of

297 IFN-γ. These data are consistent with the fact that MTBC strain CDC1551, responsible for one of the
298 most studied L4 outbreaks, was characterized by very large skin test responses in infected subjects
299 and a robust pro-inflammatory immune response in mice and in human monocytes (Manca et al.,
300 1999). In addition, we observed that L4, and to a lesser extent L3, promoted an increased secretion
301 of IL-1β. Romagnoli and collaborators showed that higher IL-1β levels trigger autophagy; however,
302 L4 isolates evade subsequent lysosomal degradation (Romagnoli et al., 2018). Despite its protective
303 role (Mayer-Barber et al., 2010), increased IL-1β levels in the bronchoalveolar lavage or serum of TB
304 patients have been associated with presence of cavities and higher bacterial loads in sputum (Sigal
305 et al., 2017; Tsao et al., 2000). Consonantly, high transmission strains induced an increased
306 expression of IL-1β in the lungs of infected mice compared to low transmission ones (Lovey et al.,
307 2022). Therefore, our and others' findings indicate that L4 constitutes an example of impeded pro-
308 inflammatory responses not to be the only way for the MTBC members to achieve global success.
309 Lastly, L3 was characterized by a tendency to preferentially remain in a metabolically active state, in
310 contrast with the increased propensity of L2 to enter dormancy, which was previously reported
311 under standard culture conditions in broth (Reed et al., 2007). Whilst it was originally thought that
312 this phenotype could be responsible for the increased virulence displayed by L2 Beijing strain in the
313 mouse model, subsequent studies disproved this hypothesis (Domenech et al., 2017). In line with
314 this, our results show that even in the context of hypoxic granulomatous responses –which are
315 lacking in the mouse model– there was no correlation between the propensity to switch into a
316 dormant state and virulence, as reflected in bacterial burden in our model, across MTBC lineages.
317 Last but not least, we have identified immune response traits that correlate with the hampered
318 mycobacterial proliferation exhibited by various MTBC strains of independent lineages. T cells are
319 essential for immunity against the MTBC (Kaufmann, 2002); hence, it is unsurprising that the level
320 of CD4 and CD8 T cell activation inversely correlated with mycobacterial growth rate. Increased levels
321 of CXCL9, granzyme B and TNF-α were also found to be associated with a better control of MTBC
322 proliferation. Among the identified soluble factors, the prominent protective role of TNF-α in TB is
323 well-known (Flynn et al., 1995). CXCL9's paradigmatic function is directing the migration of CXCR3-
324 expressing cells (i.e., T helper 1 CD4 T cells, effector CD8 T cells and natural killer cells) (Groom and
325 Luster, 2011). CXCL9 has attracted attention as potential biomarker for TB diagnosis and treatment
326 monitoring (Ambreen et al., 2021; Uzorka et al., 2022). However, some evidence suggests that CXCR3
327 ligands play a role in the positioning of effector cells within the lung for control of MTB proliferation.
328 Protective vaccination in mice triggered the production of chemokines, including CXCL9, in the lung
329 and associated recruitment of $CXCR3^+$ CD4 T cells (Khader et al., 2007). In addition, increased

330 densities of CXCR3$^+$ CD4 T cells were found in the lungs of latently infected non-human primates
331 (NHPs) relative to those with active TB (Shanmugasundaram et al., 2020). CXCL9 has also been
332 reported as a new marker of trained immunity in mycobacterial growth inhibition assays (Joosten et
333 al., 2018). Recently MTBC-exposed individuals, which exhibited the strongest control of
334 mycobacterial proliferation, produced increased levels of CXCL9. Notably, our findings are in line
335 with recent reports highlighting an important role of granzyme B in the control of MTBC infection in
336 the early stages of TB. In NHPs, low burden granulomas were associated with a higher proportion of
337 a T/NK cell cluster expressing granzyme B (Gideon et al., 2022). Furthermore, individuals with latent
338 TB infection exhibited increased expression of granzyme B in activated NK cells (Esaulova et al.,
339 2021). We did not find any correlation between IFN-γ levels and mycobacterial replication rate. Our
340 finding is supported by TB vaccine trials demonstrating that induction of strong IFN-γ responses does
341 not translate into enhanced protection (Tameris et al., 2013). However, strains with low replication
342 rates were among those inducing high IFN-γ levels. These results therefore suggest that IFN-γ is
343 required, yet not sufficient to mediate protection.
344 In summary, our investigation exposed various features that associate with certain MTBC lineages
345 and/or strains, thereby reinforcing the concept that effective treatments and vaccines need to be
346 tailored. We advocate *in vitro* granuloma models as relevant tools to understand the implications of
347 MTBC strain diversity on the interaction with humans of diverse genetic backgrounds and to assess
348 protective traits elicited by vaccines.
349
350 **MATERIALS AND METHODS**
351 **Isolation of human peripheral blood mononuclear cells (PBMCs)**
352 Buffy coats from healthy, anonymous blood donors (under informed consent) were purchased from
353 the Interregionale Blutspende SRK AG (Bern, Switzerland). PBMCs were isolated from buffy coats by
354 Ficoll-Paque (GE Healthcare) density-gradient and washed twice with RPMI-1640 with L-glutamine
355 (RPMI; Sigma-Aldrich). Aliquots were cryopreserved in RPMI supplemented with 10% DMSO (Sigma-
356 Aldrich) and 40% fetal bovine serum (FBS; Gibco) and stored in liquid nitrogen. Isolated PBMCs were
357 systematically tested for CD4 T cell reactivity against PPD (purified protein derivative; Statens Serum
358 Institute, RT23) as previously reported by our laboratory (Arbues et al., 2020a). Prior to use, PBMCs
359 from PPD-reactive donors were thawed, washed twice in RPMI containing 10% FBS (RPMI-FBS) and
360 benzonase (12.5 U/ml; BioVision) and rested in RPMI-FBS overnight at 37°C-5% CO_2. Trypan blue dye
361 exclusion method was used to confirm sample viability of above 95%. PBMC concentration was
362 adjusted to 10^7 cells/ml in RPMI supplemented with 20% human AB serum (PAN-Biotech) (RPMI-

363 HS).

364 **Culture and preparation of disperse suspensions of *M. tuberculosis* complex (MTBC) strains**

365 We selected 14 isolates (Table 1) from a reference set of clinical strains covering much of the global
366 diversity of the human-adapted MTBC (Borrell et al., 2019). This strain collection comprises drug-
367 susceptible strains isolated from patients of diverse origin that can be successfully grown in culture.
368 The strain subset used encompasses three strains per lineage for L1 to L4 and two L5 strains. The
369 laboratory strain H37Rv, which was used for the implementation of the model (Arbues et al., 2020a),
370 was included as a reference. We excluded L6 from the present study due to its characteristic
371 significantly slower growth in axenic culture (Gehre et al., 2013). L7 to L9 were not included since
372 they have only been described recently and the number of available isolates is very scarce.

373 MTBC strains were cultured under gentle agitation in Middlebrook 7H9 broth supplemented with
374 10% ADC (5% bovine albumin fraction V, 2% dextrose and 0.003% catalase), 0.5% glycerol (PanReac
375 AppliChem) and 0.05% Tween-80 (Sigma-Aldrich), additionally enriched with 40 mM sodium
376 pyruvate (Sigma-Aldrich) for L5 strains. Upon reaching mid-exponential phase (OD_{600} between 0.4
377 and 0.8), bacteria were washed with PBS containing 0.1% Tween-80 (PBST) and resuspended in
378 RPMI-FBS. The resultant mycobacterial suspension was dispersed by water-bath sonication (XUB5,
379 Grant Instruments) for 2 min, and then centrifuged at 260 $\times g$ for 5 min. The upper part of the
380 supernatant was recovered and cryopreserved by adding 5% glycerol (final) and stored at –80°C.
381 Concentration of the frozen stocks was quantified by colony forming unit (CFU) assessment (see
382 below).

383 **Generation and quantification of three-dimensional (3D) *in vitro* granulomas**

384 PBMCs from four healthy blood donors were infected independently with the selected MTBC
385 isolates, and subsequently embedded within an extracellular matrix (ECM) composed of collagen
386 and fibronectin, the main components of the lung extracellular matrix, as previously reported
387 (Arbues et al., 2020b). Briefly, an ECM solution composed of 950 μl/ml of collagen (PureCol, 3
388 mg/ml; Advanced BioMatrix), 50 μl/ml of PBS 10X, 4 μl/ml of human fibronectin (1 mg/ml; Sigma-
389 Aldrich), and 10 μl of 1 N NaOH (Sigma-Aldrich) was prepared and incubated at 4°C for 90 min.
390 Rested PBMCs were infected with the various MTBC strains at a multiplicity of infection (MOI) of
391 1:200 (bacteria:PBMCs), or left uninfected when required. Thereafter, 1.25×10^6 PBMCs per well
392 were distributed across 48-well plates and mixed with the pre-incubated ECM in a 1:1 (v/v) ratio.
393 The ECM was left to set for 45 min at 37°C-5% CO_2 before 250 μl of RPMI-HS were added.

394 Granuloma formation was monitored on day 7 post-infection using a Leica THUNDER Imager Live
395 Cell (Leica). Cellular aggregates present in a representative bright field per donor and condition were

396 enumerated and measured using ImageJ 1.52n (National Institutes of Health, US). The total number
397 of granulomas, their size and aspect ratio (i.e., the ratio of the major axis to the minor axis; and so,
398 and aspect ratio of 1 corresponds to a circle, and >1 to an ellipse) were integrated into a granuloma
399 score as follows: the area of each individual granuloma was divided by its corresponding aspect ratio,
400 then the average was calculated and divided by the total number of aggregates.

401 $$Granuloma\ score\ = \frac{\overline{X}\ (granuloma\ area/aspect\ ratio)}{No.\ aggregates}$$

402 Thus, the induction of numerous but small aggregates with an elongated shape translates into the
403 lowest granuloma scores; whilst generation of bigger, even if fewer, circular aggregates results in
404 higher values.

405 **Retrieval of mycobacteria**

406 At the relevant time points, supernatant was removed and the ECM was digested with 125 μl of
407 collagenase (1 mg/ml; Sigma-Aldrich) for 40 min at 37°C-5% CO2. Subsequently, host cells were lysed
408 by adding 125 μl of 0.4% Triton X-100 (Sigma-Aldrich) and incubating for 20 min at room
409 temperature. Released bacilli were subsequently used for bacterial load quantification by CFU
410 assessment and dual auramine-O/Nile red staining.

411 **CFU assessment**

412 Briefly, 10-fold serial dilutions of the mycobacterial suspensions were prepared in triplicate in PBST
413 and plated on 7H11 agar (BBL) plates supplemented with 0.5% glycerol and 10% OADC (0.05% oleic
414 acid in ADC), additionally enriched with 40 mM sodium pyruvate for L5 strains. Plates were incubated
415 at 37°C-5% CO_2 for 3-4 weeks.

416 **Dual auramine-O/Nile red staining**

417 Bacilli retrieved on day 7 post-infection were inactivated with 1X CellFIX (BD) for 20 min at room
418 temperature and afterwards stored at 4°C until processing. Fixed samples were centrifuged at 10,000
419 ×*g* for 5 min to remove the fixative prior being resuspended in water. Subsequently they were
420 spotted on glass slides, air dried and heat fixed at 70°C. Fluorescent acid-fast staining using TB
421 Fluorescent Stain Kit M (BD) was performed in combination with neutral-lipid staining dye Nile red
422 (Sigma) (Arbues et al., 2020a). Briefly, each sample was stained with auramine-O for 20 min,
423 decolorized for 30 s, covered with Nile red (10 μg/ml) for 15 min and counterstained with potassium
424 permanganate for 2 min, including gentle washes with distilled water between each step. Air-dried,
425 stained slides were mounted using Vectashield mounting medium (Vectorlabs) and examined using
426 a Leica DM5000 B fluorescence microscope (Leica). For quantification purposes, at least 200 bacteria
427 per sample were counted manually.

428 **Macrophage cell death quantification**

429 On day 6 post-infection, cells were released from the ECM by collagenase digestion as described
430 above. Subsequently, they were pelleted at 400 ×*g* for 5 min and extracellularly stained as follows.
431 Cells were incubated for 15 min at room temperature in 100 μl of Annexin binding buffer (ABB,
432 BioLegend) containing APC-labeled Annexin V, 7-AAD, and fluorochrome-labeled antibodies
433 (BioLegend) against human CD3 (Pacific blue, clone UCHT1), CD19 (BV510, clone HIB19), and CD11b
434 (PE-Cy7, clone ICRF44). Samples were washed once with ABB and fixed in 1X CellFIX (BD) for 20 min
435 at room temperature. Samples were acquired on a MACSQuant Analyzer 10 (Miltenyi Biotec) and
436 processed using FlowJo 10.6.1 (BD).

437 **Assessment of lymphocyte activation and proliferation**

438 Prior to infection for the generation of 3D *in vitro* granulomas, rested PBMCs were labeled with
439 carboxyfluorescein succinimidyl ester (CFSE). Briefly, PBMCs were resuspended in PBS containing
440 1 μM CFSE (BioLegend) at 5×10^6 cells/ml and incubated at 37°C-5% CO_2 for 10 min. After quenching
441 the staining by adding 2.5 volumes of PBS containing 20% FBS, cells were pelleted and resuspended
442 at 10^7 cells/ml in RPMI-HS.

443 On day 6 post-infection, cells were released from the ECM by collagenase digestion as described
444 above. Subsequently, they were pelleted at 400 ×*g* for 5 min and extracellularly stained following a
445 standard protocol. Cells were incubated for 20 min at room temperature in 100 μl of FACS buffer
446 (0.1% FBS in PBS) containing fluorochrome-labeled antibodies (BioLegend) against human CD3
447 (Pacific blue, clone UCHT1), CD4 (PE-Cy7, clone RPA-T4), CD8 (BV510, clone HIT8a), CD19 (BV510,
448 clone HIB19), CD25 (PE, clone BC96), CD69 (PerCP, clone FN50), CD38 (APC, clone HIT2), and HLA-
449 DR (APC-Cy7, clone L243). Samples were washed once with FACS buffer and fixed in fixation buffer
450 (BioLegend) for 20 min at room temperature. Samples were acquired on a MACSQuant Analyzer 10
451 (Miltenyi Biotec) and processed using FlowJo 10.6.1 (BD).

452 **Quantification of soluble factors**

453 Supernatants collected on day 1 and 8 post-infection, and stored at –80°C in the meantime, were
454 filter-sterilized no more than 24 h prior to analysis by multiplex bead-based immunoassay. A
455 ProcartaPlex custom panel (including CCL2/MCP-1, CCL3/MIP-1α, CXCL9/MIG, TNF-α, IL-1β, IL-2, IL-
456 6, IL-10, IL-12p70, IL-13, IFN-α, IFN-γ, GM-CSF, granzyme B and MMP-1) (Invitrogen) and the Bio-Plex
457 Pro™ human Th17 cytokine panel (Bio-Rad) (including IL-17A, IL-17F, IL-21, IL-22 and IL-23) were
458 used according to the manufacturer's recommendations and acquired on a Luminex Bio-Plex 200
459 platform and Bio-Plex Manager 6.0 software (Bio-Rad). Culture medium was measured in parallel to
460 the samples to assess any potential residual presence of the target biomolecules in the human

461 serum. Results were analyzed using R package nCal (Fong et al., 2013).

462 **Quantification and statistical analysis**

463 GraphPad Prism 8.2.1 and R.4.3.1 and R studio 2023.06.1-524 were used to produce quantitative
464 graphical representations of the generated data and to perform statistical analyses. The nature of
465 the tests and definition of center and significance levels is specified within the respective figure
466 legend.

467

468 **FUNDING**

469 This work was supported by the Swiss National Science Foundation (SNSF198838).

470

471 **AUTHOR CONTRIBUTIONS**

472 Conceptualization, A.A. and D.P.; Methodology, A.A., S.S., and D.P.; Investigation, A.A., S.S., and M.R.;
473 Formal analysis, Visualization, A.A, S.S. and D.P.; Writing – Original Draft, A.A, S.S. and D.P.; Writing
474 – Review & Editing, A.A., S.S., S.B., S.G. and D.P.; Funding Acquisition, D.P.; and Supervision, D.P.
475 The authors declare no competing interests.

476

477 **REFERENCES**

478 Aguilo, J.I., Alonso, H., Uranga, S., Marinova, D., Arbues, A., de Martino, A., Anel, A., Monzon, M.,
479 Badiola, J., Pardo, J.*, et al.* (2013). ESX-1-induced apoptosis is involved in cell-to-cell spread of
480 Mycobacterium tuberculosis. Cell Microbiol *15*, 1994-2005.

481 Ambreen, A., Khaliq, A., Naqvi, S.Z.H., Tahir, A., Mustafa, M., Chaudhary, S.U., Mirza, S., and Mustafa,
482 T. (2021). Host biomarkers for monitoring therapeutic response in extrapulmonary tuberculosis.
483 Cytokine *142*, 155499.

484 Arbues, A., Brees, D., Chibout, S.D., Fox, T., Kammuller, M., and Portevin, D. (2020a). TNF-alpha
485 antagonists differentially induce TGF-beta1-dependent resuscitation of dormant-like
486 Mycobacterium tuberculosis. PLoS Pathog *16*, e1008312.

487 Arbues, A., Kammuller, M., and Portevin, D. (2020b). Generating Three-dimensional Human
488 Granulomas in vitro to Study Mycobacterium tuberculosis-Host Interaction. Bio Protoc *10*, e3820.

489 Arbues, A., Schmidiger, S., Kammuller, M., and Portevin, D. (2021). Extracellular Matrix-Induced GM-
490 CSF and Hypoxia Promote Immune Control of Mycobacterium tuberculosis in Human In Vitro
491 Granulomas. Front Immunol *12*, 727508.

492 Asante-Poku, A., Yeboah-Manu, D., Otchere, I.D., Aboagye, S.Y., Stucki, D., Hattendorf, J., Borrell, S.,
493 Feldmann, J., Danso, E., and Gagneux, S. (2015). Mycobacterium africanum is associated with patient

494 ethnicity in Ghana. PLoS Negl Trop Dis *9*, e3370.
495 Ates, L.S., Dippenaar, A., Sayes, F., Pawlik, A., Bouchier, C., Ma, L., Warren, R.M., Sougakoff, W.,
496 Majlessi, L., van Heijst, J.W.J.*, et al.* (2018). Unexpected Genomic and Phenotypic Diversity of
497 Mycobacterium africanum Lineage 5 Affects Drug Resistance, Protein Secretion, and
498 Immunogenicity. Genome Biol Evol *10*, 1858-1874.
499 Borrell, S., Trauner, A., Brites, D., Rigouts, L., Loiseau, C., Coscolla, M., Niemann, S., De Jong, B.,
500 Yeboah-Manu, D., Kato-Maeda, M.*, et al.* (2019). Reference set of Mycobacterium tuberculosis
501 clinical strains: A tool for research and product development. PLoS One *14*, e0214088.
502 Bottai, D., Frigui, W., Sayes, F., Di Luca, M., Spadoni, D., Pawlik, A., Zoppo, M., Orgeur, M., Khanna,
503 V., Hardy, D.*, et al.* (2020). TbD1 deletion as a driver of the evolutionary success of modern epidemic
504 Mycobacterium tuberculosis lineages. Nat Commun *11*, 684.
505 Brosch, R., Gordon, S.V., Marmiesse, M., Brodin, P., Buchrieser, C., Eiglmeier, K., Garnier, T., Gutierrez,
506 C., Hewinson, G., Kremer, K.*, et al.* (2002). A new evolutionary scenario for the Mycobacterium
507 tuberculosis complex. Proc Natl Acad Sci U S A *99*, 3684-3689.
508 Caws, M., Thwaites, G., Dunstan, S., Hawn, T.R., Lan, N.T., Thuong, N.T., Stepniewska, K., Huyen, M.N.,
509 Bang, N.D., Loc, T.H.*, et al.* (2008). The influence of host and bacterial genotype on the development
510 of disseminated disease with Mycobacterium tuberculosis. PLoS Pathog *4*, e1000034.
511 Click, E.S., Moonan, P.K., Winston, C.A., Cowan, L.S., and Oeltmann, J.E. (2012). Relationship
512 between Mycobacterium tuberculosis phylogenetic lineage and clinical site of tuberculosis. Clin
513 Infect Dis *54*, 211-219.
514 Coll, F., McNerney, R., Guerra-Assuncao, J.A., Glynn, J.R., Perdigao, J., Viveiros, M., Portugal, I., Pain,
515 A., Martin, N., and Clark, T.G. (2014). A robust SNP barcode for typing Mycobacterium tuberculosis
516 complex strains. Nat Commun *5*, 4812.
517 Comas, I., Coscolla, M., Luo, T., Borrell, S., Holt, K.E., Kato-Maeda, M., Parkhill, J., Malla, B., Berg, S.,
518 Thwaites, G.*, et al.* (2013). Out-of-Africa migration and Neolithic coexpansion of Mycobacterium
519 tuberculosis with modern humans. Nat Genet *45*, 1176-1182.
520 Coscolla, M., Gagneux, S., Menardo, F., Loiseau, C., Ruiz-Rodriguez, P., Borrell, S., Otchere, I.D.,
521 Asante-Poku, A., Asare, P., Sanchez-Buso, L.*, et al.* (2021). Phylogenomics of Mycobacterium
522 africanum reveals a new lineage and a complex evolutionary history. Microb Genom *7*.
523 Davis, J.M., and Ramakrishnan, L. (2009). The role of the granuloma in expansion and dissemination
524 of early tuberculous infection. Cell *136*, 37-49.
525 Domenech, P., Kolly, G.S., Leon-Solis, L., Fallow, A., and Reed, M.B. (2010). Massive gene duplication
526 event among clinical isolates of the Mycobacterium tuberculosis W/Beijing family. J Bacteriol *192*,

527 4562-4570.
528 Domenech, P., Zou, J., Averback, A., Syed, N., Curtis, D., Donato, S., and Reed, M.B. (2017). Unique
529 Regulation of the DosR Regulon in the Beijing Lineage of Mycobacterium tuberculosis. J Bacteriol
530 *199*.
531 Esaulova, E., Das, S., Singh, D.K., Choreno-Parra, J.A., Swain, A., Arthur, L., Rangel-Moreno, J., Ahmed,
532 M., Singh, B., Gupta, A.*, et al.* (2021). The immune landscape in tuberculosis reveals populations
533 linked to disease and latency. Cell Host Microbe *29*, 165-178 e168.
534 Flynn, J.L., Goldstein, M.M., Chan, J., Triebold, K.J., Pfeffer, K., Lowenstein, C.J., Schreiber, R., Mak,
535 T.W., and Bloom, B.R. (1995). Tumor necrosis factor-alpha is required in the protective immune
536 response against Mycobacterium tuberculosis in mice. Immunity *2*, 561-572.
537 Fong, Y., Sebestyen, K., Yu, X., Gilbert, P., and Self, S. (2013). nCal: an R package for non-linear
538 calibration. Bioinformatics *29*, 2653-2654.
539 Gagneux, S., DeRiemer, K., Van, T., Kato-Maeda, M., de Jong, B.C., Narayanan, S., Nicol, M., Niemann,
540 S., Kremer, K., Gutierrez, M.C.*, et al.* (2006). Variable host-pathogen compatibility in Mycobacterium
541 tuberculosis. Proc Natl Acad Sci U S A *103*, 2869-2873.
542 Garton, N.J., Waddell, S.J., Sherratt, A.L., Lee, S.M., Smith, R.J., Senner, C., Hinds, J., Rajakumar, K.,
543 Adegbola, R.A., Besra, G.S.*, et al.* (2008). Cytological and transcript analyses reveal fat and lazy
544 persister-like bacilli in tuberculous sputum. PLoS Med *5*, e75.
545 Gehre, F., Otu, J., DeRiemer, K., de Sessions, P.F., Hibberd, M.L., Mulders, W., Corrah, T., de Jong, B.C.,
546 and Antonio, M. (2013). Deciphering the growth behaviour of Mycobacterium africanum. PLoS Negl
547 Trop Dis *7*, e2220.
548 Gengenbacher, M., and Kaufmann, S.H. (2012). Mycobacterium tuberculosis: success through
549 dormancy. FEMS Microbiol Rev *36*, 514-532.
550 Gideon, H.P., Hughes, T.K., Tzouanas, C.N., Wadsworth, M.H., 2nd, Tu, A.A., Gierahn, T.M., Peters,
551 J.M., Hopkins, F.F., Wei, J.R., Kummerlowe, C.*, et al.* (2022). Multimodal profiling of lung granulomas
552 in macaques reveals cellular correlates of tuberculosis control. Immunity *55*, 827-846 e810.
553 Groom, J.R., and Luster, A.D. (2011). CXCR3 ligands: redundant, collaborative and antagonistic
554 functions. Immunol Cell Biol *89*, 207-215.
555 Guerra-Assuncao, J.A., Crampin, A.C., Houben, R.M., Mzembe, T., Mallard, K., Coll, F., Khan, P., Banda,
556 L., Chiwaya, A., Pereira, R.P.*, et al.* (2015). Large-scale whole genome sequencing of M. tuberculosis
557 provides insights into transmission in a high prevalence area. Elife *4*.
558 Guyeux, C., Senelle, G., Le Meur, A., Supply, P., Gaudin, C., Phelan, J.E., Clark, T.G., Rigouts, L., de
559 Jong, B., Sola, C.*, et al.* (2024). Newly Identified Mycobacterium africanum Lineage 10, Central Africa.

560 Emerg Infect Dis *30*, 560-563.
561 Hiza, H., Zwyer, M., Hella, J., Arbués, A., Sasamalo, M., Borrell, S., Xu, Z.M., Ross, A., Brites, D., Fellay,
562 J.*, et al.* (2023). Bacterial diversity dominates variable macrophage responses of tuberculosis
563 patients in Tanzania. bioRxiv.
564 Joosten, S.A., van Meijgaarden, K.E., Arend, S.M., Prins, C., Oftung, F., Korsvold, G.E., Kik, S.V., Arts,
565 R.J., van Crevel, R., Netea, M.G.*, et al.* (2018). Mycobacterial growth inhibition is associated with
566 trained innate immunity. J Clin Invest *128*, 1837-1851.
567 Kaufmann, S.H. (2002). Protection against tuberculosis: cytokines, T cells, and macrophages. Ann
568 Rheum Dis *61 Suppl 2*, ii54-58.
569 Khader, S.A., Bell, G.K., Pearl, J.E., Fountain, J.J., Rangel-Moreno, J., Cilley, G.E., Shen, F., Eaton, S.M.,
570 Gaffen, S.L., Swain, S.L.*, et al.* (2007). IL-23 and IL-17 in the establishment of protective pulmonary
571 CD4+ T cell responses after vaccination and during Mycobacterium tuberculosis challenge. Nat
572 Immunol *8*, 369-377.
573 Lovey, A., Verma, S., Kaipilyawar, V., Ribeiro-Rodrigues, R., Husain, S., Palaci, M., Dietze, R., Ma, S.,
574 Morrison, R.D., Sherman, D.R.*, et al.* (2022). Early alveolar macrophage response and IL-1R-
575 dependent T cell priming determine transmissibility of Mycobacterium tuberculosis strains. Nat
576 Commun *13*, 884.
577 Manca, C., Tsenova, L., Barry, C.E., 3rd, Bergtold, A., Freeman, S., Haslett, P.A., Musser, J.M.,
578 Freedman, V.H., and Kaplan, G. (1999). Mycobacterium tuberculosis CDC1551 induces a more
579 vigorous host response in vivo and in vitro, but is not more virulent than other clinical isolates. J
580 Immunol *162*, 6740-6746.
581 Manca, C., Tsenova, L., Bergtold, A., Freeman, S., Tovey, M., Musser, J.M., Barry, C.E., 3rd, Freedman,
582 V.H., and Kaplan, G. (2001). Virulence of a Mycobacterium tuberculosis clinical isolate in mice is
583 determined by failure to induce Th1 type immunity and is associated with induction of IFN-alpha
584 /beta. Proc Natl Acad Sci U S A *98*, 5752-5757.
585 Mayer-Barber, K.D., Barber, D.L., Shenderov, K., White, S.D., Wilson, M.S., Cheever, A., Kugler, D.,
586 Hieny, S., Caspar, P., Nunez, G.*, et al.* (2010). Caspase-1 independent IL-1beta production is critical
587 for host resistance to mycobacterium tuberculosis and does not require TLR signaling in vivo. J
588 Immunol *184*, 3326-3330.
589 Mitchison, D.A., Wallace, J.G., Bhatia, A.L., Selkon, J.B., Subbaiah, T.V., and Lancaster, M.C. (1960). A
590 comparison of the virulence in guinea-pigs of South Indian and British tubercle bacilli. Tubercle *41*,
591 1-22.
592 Moreira-Teixeira, L., Tabone, O., Graham, C.M., Singhania, A., Stavropoulos, E., Redford, P.S.,

593 Chakravarty, P., Priestnall, S.L., Suarez-Bonnet, A., Herbert, E.*, et al.* (2020). Mouse transcriptome
594 reveals potential signatures of protection and pathogenesis in human tuberculosis. Nat Immunol *21*,
595 464-476.
596 Napier, G., Campino, S., Merid, Y., Abebe, M., Woldeamanuel, Y., Aseffa, A., Hibberd, M.L., Phelan,
597 J., and Clark, T.G. (2020). Robust barcoding and identification of Mycobacterium tuberculosis
598 lineages for epidemiological and clinical studies. Genome Med *12*, 114.
599 Nebenzahl-Guimaraes, H., Verhagen, L.M., Borgdorff, M.W., and van Soolingen, D. (2015).
600 Transmission and Progression to Disease of Mycobacterium tuberculosis Phylogenetic Lineages in
601 The Netherlands. J Clin Microbiol *53*, 3264-3271.
602 Netikul, T., Palittapongarnpim, P., Thawornwattana, Y., and Plitphonganphim, S. (2021). Estimation
603 of the global burden of Mycobacterium tuberculosis lineage 1. Infect Genet Evol *91*, 104802.
604 Newton, S.M., Smith, R.J., Wilkinson, K.A., Nicol, M.P., Garton, N.J., Staples, K.J., Stewart, G.R., Wain,
605 J.R., Martineau, A.R., Fandrich, S.*, et al.* (2006). A deletion defining a common Asian lineage of
606 Mycobacterium tuberculosis associates with immune subversion. Proc Natl Acad Sci U S A *103*,
607 15594-15598.
608 Ofori-Anyinam, B., Dolganov, G., Van, T., Davis, J.L., Walter, N.D., Garcia, B.J., Voskuil, M., Fissette, K.,
609 Diels, M., Driesen, M.*, et al.* (2017). Significant under expression of the DosR regulon in M.
610 tuberculosis complex lineage 6 in sputum. Tuberculosis (Edinb) *104*, 58-64.
611 Osei-Wusu, S., Tetteh, J.K.A., Musah, A.B., Ntiamoah, D.O., Arthur, N., Adjei, A., Arbues, A., Ofori,
612 E.A., Mensah, K.A., Galevo, S.E.A.*, et al.* (2023). Macrophage susceptibility to infection by Ghanaian
613 Mycobacterium tuberculosis complex lineages 4 and 5 varies with self-reported ethnicity. Front Cell
614 Infect Microbiol *13*, 1163993.
615 Pagan, A.J., and Ramakrishnan, L. (2014). Immunity and Immunopathology in the Tuberculous
616 Granuloma. Cold Spring Harb Perspect Med *5*.
617 Perez, I., Uranga, S., Sayes, F., Frigui, W., Samper, S., Arbues, A., Aguilo, N., Brosch, R., Martin, C., and
618 Gonzalo-Asensio, J. (2020). Live attenuated TB vaccines representing the three modern
619 Mycobacterium tuberculosis lineages reveal that the Euro-American genetic background confers
620 optimal vaccine potential. EBioMedicine *55*, 102761.
621 Plumlee, C.R., Duffy, F.J., Gern, B.H., Delahaye, J.L., Cohen, S.B., Stoltzfus, C.R., Rustad, T.R., Hansen,
622 S.G., Axthelm, M.K., Picker, L.J.*, et al.* (2021). Ultra-low Dose Aerosol Infection of Mice with
623 Mycobacterium tuberculosis More Closely Models Human Tuberculosis. Cell Host Microbe *29*, 68-82
624 e65.
625 Poonawala, H., Kumar, N., and Peacock, S.J. (2020). A review of published spoligotype data indicates

626 the diversity of Mycobacterium tuberculosis from India is under-represented in global databases.
627 Infect Genet Evol *78*, 104072.
628 Portevin, D., Gagneux, S., Comas, I., and Young, D. (2011). Human macrophage responses to clinical
629 isolates from the Mycobacterium tuberculosis complex discriminate between ancient and modern
630 lineages. PLoS Pathog *7*, e1001307.
631 Reed, M.B., Domenech, P., Manca, C., Su, H., Barczak, A.K., Kreiswirth, B.N., Kaplan, G., and Barry,
632 C.E., 3rd (2004). A glycolipid of hypervirulent tuberculosis strains that inhibits the innate immune
633 response. Nature *431*, 84-87.
634 Reed, M.B., Gagneux, S., Deriemer, K., Small, P.M., and Barry, C.E., 3rd (2007). The W-Beijing lineage
635 of Mycobacterium tuberculosis overproduces triglycerides and has the DosR dormancy regulon
636 constitutively upregulated. J Bacteriol *189*, 2583-2589.
637 Reiling, N., Homolka, S., Walter, K., Brandenburg, J., Niwinski, L., Ernst, M., Herzmann, C., Lange, C.,
638 Diel, R., Ehlers, S.*, et al.* (2013). Clade-specific virulence patterns of Mycobacterium tuberculosis
639 complex strains in human primary macrophages and aerogenically infected mice. mBio *4*.
640 Ribeiro, S.C., Gomes, L.L., Amaral, E.P., Andrade, M.R., Almeida, F.M., Rezende, A.L., Lanes, V.R.,
641 Carvalho, E.C., Suffys, P.N., Mokrousov, I.*, et al.* (2014). Mycobacterium tuberculosis strains of the
642 modern sublineage of the Beijing family are more likely to display increased virulence than strains
643 of the ancient sublineage. J Clin Microbiol *52*, 2615-2624.
644 Romagnoli, A., Petruccioli, E., Palucci, I., Camassa, S., Carata, E., Petrone, L., Mariano, S., Sali, M.,
645 Dini, L., Girardi, E.*, et al.* (2018). Clinical isolates of the modern Mycobacterium tuberculosis lineage
646 4 evade host defense in human macrophages through eluding IL-1beta-induced autophagy. Cell
647 Death Dis *9*, 624.
648 Saelens, J.W., Sweeney, M.I., Viswanathan, G., Xet-Mull, A.M., Jurcic Smith, K.L., Sisk, D.M., Hu, D.D.,
649 Cronin, R.M., Hughes, E.J., Brewer, W.J.*, et al.* (2022). An ancestral mycobacterial effector promotes
650 dissemination of infection. Cell *185*, 4507-4525 e4518.
651 Seraphin, M.N., Doggett, R., Johnston, L., Zabala, J., Gerace, A.M., and Lauzardo, M. (2017).
652 Association between Mycobacterium tuberculosis lineage and site of disease in Florida, 2009-2015.
653 Infect Genet Evol *55*, 366-371.
654 Shanmugasundaram, U., Bucsan, A.N., Ganatra, S.R., Ibegbu, C., Quezada, M., Blair, R.V., Alvarez, X.,
655 Velu, V., Kaushal, D., and Rengarajan, J. (2020). Pulmonary Mycobacterium tuberculosis control
656 associates with CXCR3- and CCR6-expressing antigen-specific Th1 and Th17 cell recruitment. JCI
657 Insight *5*.
658 Sigal, G.B., Segal, M.R., Mathew, A., Jarlsberg, L., Wang, M., Barbero, S., Small, N., Haynesworth, K.,

659 Davis, J.L., Weiner, M.*, et al.* (2017). Biomarkers of Tuberculosis Severity and Treatment Effect: A
660 Directed Screen of 70 Host Markers in a Randomized Clinical Trial. EBioMedicine *25*, 112-121.
661 Silva, M.L., Ca, B., Osorio, N.S., Rodrigues, P.N.S., Maceiras, A.R., and Saraiva, M. (2022). Tuberculosis
662 caused by Mycobacterium africanum: Knowns and unknowns. PLoS Pathog *18*, e1010490.
663 Tameris, M., McShane, H., McClain, J.B., Landry, B., Lockhart, S., Luabeya, A.K., Geldenhuys, H., Shea,
664 J., Hussey, G., van der Merwe, L.*, et al.* (2013). Lessons learnt from the first efficacy trial of a new
665 infant tuberculosis vaccine since BCG. Tuberculosis (Edinb) *93*, 143-149.
666 Tram, T.T.B., Nhung, H.N., Vijay, S., Hai, H.T., Thu, D.D.A., Ha, V.T.N., Dinh, T.D., Ashton, P.M., Hanh,
667 N.T., Phu, N.H.*, et al.* (2018). Virulence of Mycobacterium tuberculosis Clinical Isolates Is Associated
668 With Sputum Pre-treatment Bacterial Load, Lineage, Survival in Macrophages, and Cytokine
669 Response. Front Cell Infect Microbiol *8*, 417.
670 Tsao, T.C., Hong, J., Li, L.F., Hsieh, M.J., Liao, S.K., and Chang, K.S. (2000). Imbalances between tumor
671 necrosis factor-alpha and its soluble receptor forms, and interleukin-1beta and interleukin-1
672 receptor antagonist in BAL fluid of cavitary pulmonary tuberculosis. Chest *117*, 103-109.
673 Tsenova, L., Ellison, E., Harbacheuski, R., Moreira, A.L., Kurepina, N., Reed, M.B., Mathema, B., Barry,
674 C.E., 3rd, and Kaplan, G. (2005). Virulence of selected Mycobacterium tuberculosis clinical isolates
675 in the rabbit model of meningitis is dependent on phenolic glycolipid produced by the bacilli. J Infect
676 Dis *192*, 98-106.
677 Uzorka, J.W., Bakker, J.A., van Meijgaarden, K.E., Leyten, E.M.S., Delfos, N.M., Hetem, D.J.,
678 Kerremans, J., Zwarts, M., Cozijn, S., Ottenhoff, T.H.M.*, et al.* (2022). Biomarkers to identify
679 Mycobacterium tuberculosis infection among borderline QuantiFERON results. Eur Respir J *60*.
680 Wang, C., Peyron, P., Mestre, O., Kaplan, G., van Soolingen, D., Gao, Q., Gicquel, B., and Neyrolles, O.
681 (2010). Innate immune response to Mycobacterium tuberculosis Beijing and other genotypes. PLoS
682 One *5*, e13594.
683 WHO (2023). Global Tuberculosis Report 2023 (WHO).
684

685 **Table 1. MTBC isolates used in this work**

Strain[a]		Sublineage[b]	Patient origin	Additional information
L1A	**N0069**	L1.1.1	China	
L1B	**N0072**	L1.1.2	India	
L1C	**N0157**	L.1.2.1	Philippines	
L2A	**N0031**	L2.1	China	Proto-Beijing (DRD105, RD207 present)
L2B	**N0052**	L.2.2.2	China	Ancestral Beijing (DRD105, DRD207)
L2C	**N0155**	L2.2.1	China	Modern Beijing (DRD105, DRD207, DRD181)
L3A	**N0004**	L3.1	India	
L3B	**N0054**	ND	Ethiopia	
L3C	**N1274**	L3.2	Afghanistan	
L4A	**N1216**	L4.6.2.2	Ghana	Cameroon – “Specialist”
L4B	**N0136**	L4.3.3	USA	LAM – “Generalist”
L4C	**N1283**	L4.2.1	Germany	Ural
L5A	**N1268**	L5.1	Sierra Leone	
L5B	**N1272**	L5.1.2	Ghana	

686 [a] Nomenclature used in the current study (left) and in (Borrell et al., 2019) (right). [b] Classification
687 based on (Ates et al., 2018; Coll et al., 2014; Napier et al., 2020). ND, not determined; Δ, deletion;
688 RD, region of difference.

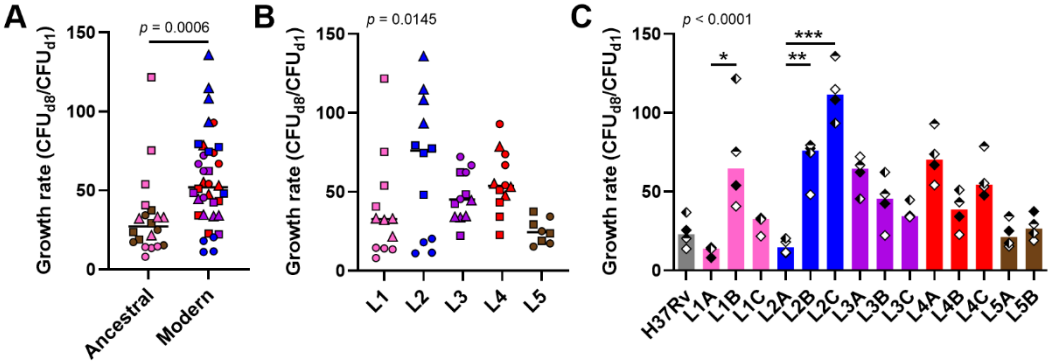

Figure 1. Mycobacterial growth in human *in vitro* granulomas shows marked intra-lineage diversity and is overall increased for MTBC modern lineages. Growth rate between days 1 and 8 p.i. stratified by **(A)** ancestral or modern lineage, **(B)** specific lineage, or **(C)** individual strain. Colors indicate lineage, and horizontal lines and bars represent medians. Shapes stand for (**A-B**) individual strains within the same lineage (LXA in circles, LXB in squares and LXC in triangles), or (**C**) independent donors. Statistical analyses by (**A**) two-tailed Mann-Whitney, (**B**) Kruskal-Wallis, or (**C**) Friedman test with *post hoc* Dunn's correction. *, $p < 0.05$; **, $p < 0.01$; ***, $p < 0.001$.

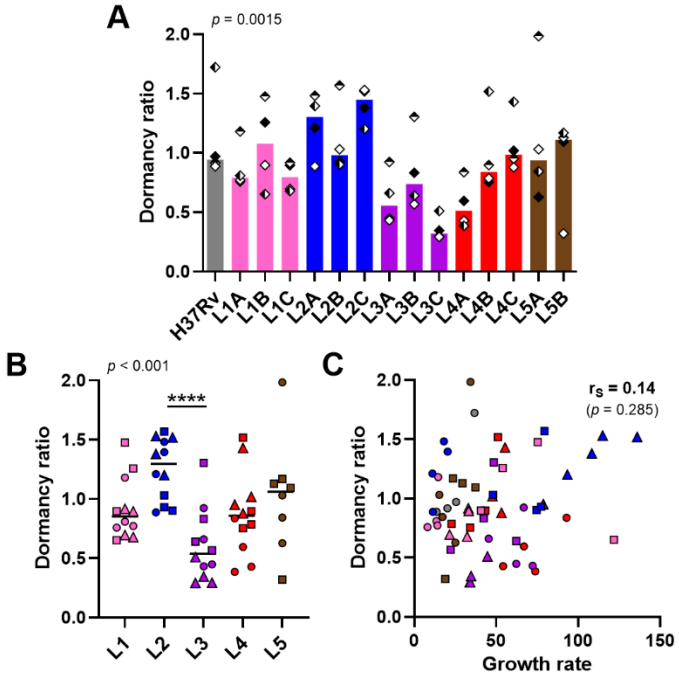

697

698 **Figure 2. Propensity to enter dormancy is particularly pronounced in lineage 2 and reduced in**
699 **lineage 3 strains.** Bacilli recovered on day 8 p.i. were stained with Auramine-O (Au) and Nile red
700 (NR). The ratio between dormant (Au^{-} NR^{+}) and metabolically active (Au^{+} NR^{-}) bacteria (dormancy
701 ratio) was quantified by fluorescence microscopy. Data stratified by **(A)** individual strain, or **(B)**
702 lineage. **(C)** Two-tailed Spearman's correlation analysis of dormancy ratio with growth rate. Colors
703 indicate lineage, and bars and horizontal lines represent medians. Shapes stand for (**A**) independent
704 donors, or (**B-C**) individual strains within the same lineage (LXA in circles, LXB in squares and LXC in
705 triangles). Statistical analyses by (**A**) Friedman, or (**B**) Kruskal-Wallis test with *post hoc* Dunn's
706 correction. ****, $p < 0.0001$.

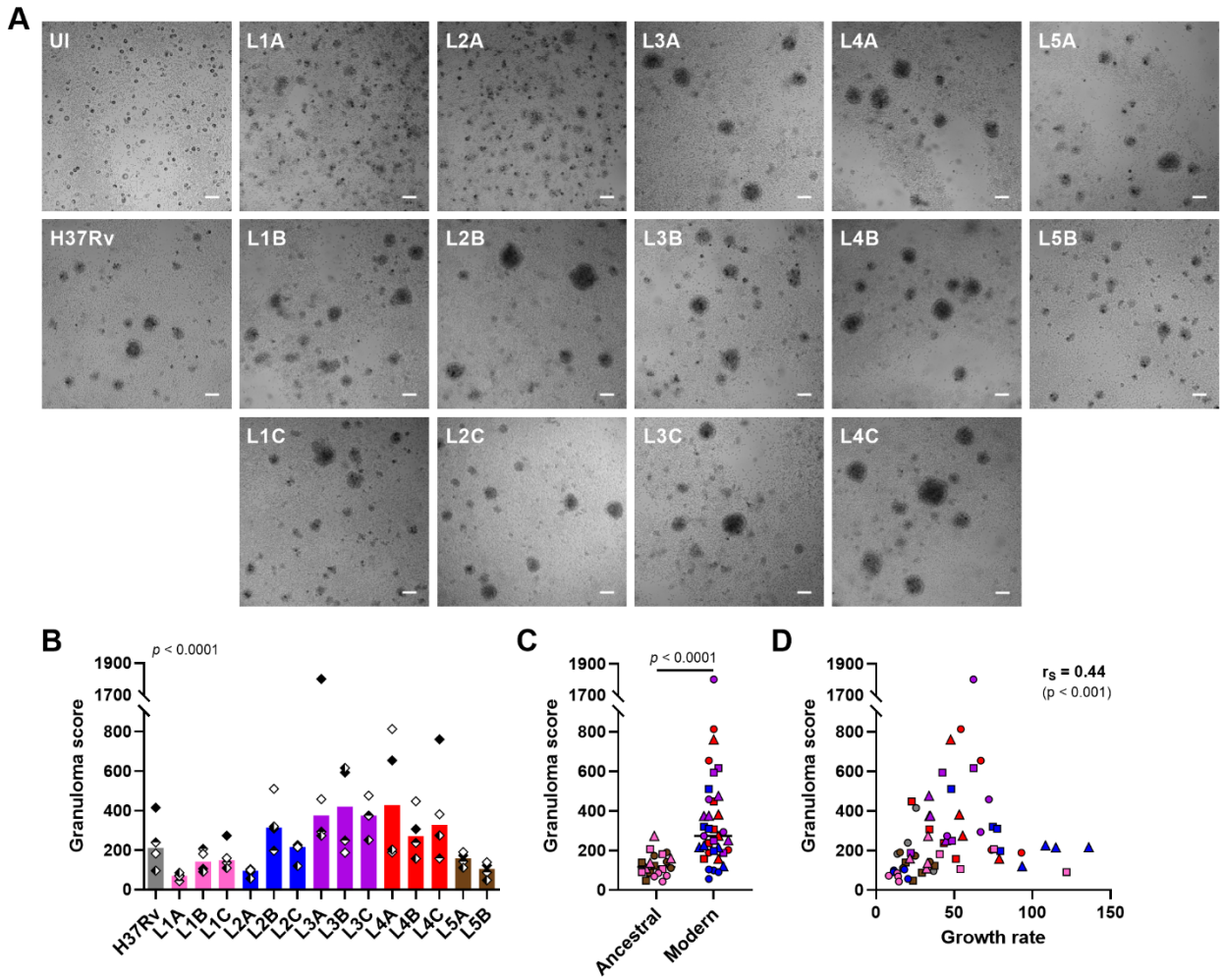

Figure 3. MTBC strain diversity translates into a spectrum of granulomatous responses that correlates with bacterial growth. (A) Bright field images of *in vitro* granulomas on day 7 p.i. from a representative donor. Scale bar = 100 µm. UI, uninfected. Number, area and aspect ratio of cell aggregates were quantified and integrated into a granuloma score (see methods). Granuloma scores stratified by **(B)** individual strain, and **(C)** ancestral or modern lineage. **(D)** Two-tailed Spearman's correlation analysis of granuloma score with growth rate. Colors indicate lineage, and bars represent medians. Shapes stand for (**B**) independent donors, or (**C-D**) individual strains within the same lineage (LXA in circles, LXB in squares and LXC in triangles). Statistical analyses by (**B**) Friedman, or (**C**) two-tailed Mann-Whitney test.

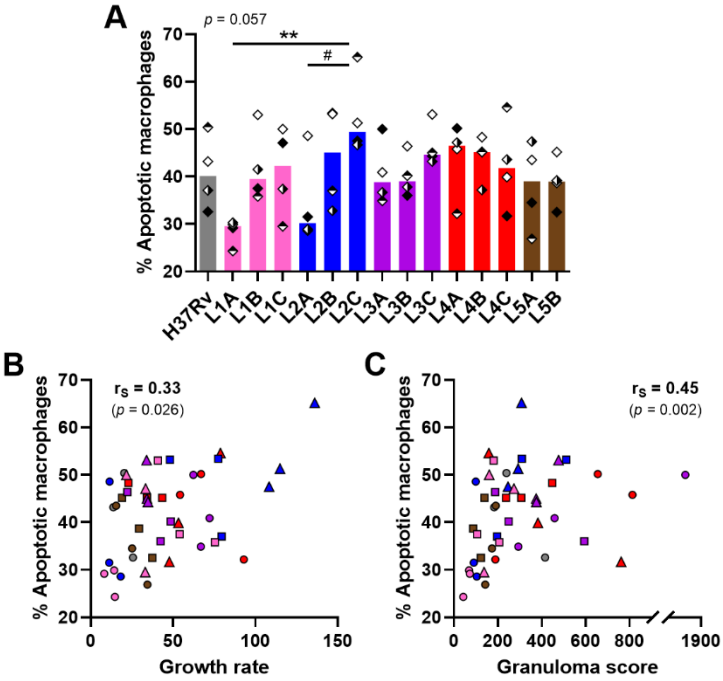

717

718 **Figure 4. Macrophage apoptosis is positively associated with mycobacterial growth rate and**
719 **granuloma score. (A)** Percentage of apoptotic macrophages (CD11b^{+} Annexin V^{+} 7-AAD^{-}) on day 6
720 p.i. quantified by flow cytometry. **(B-C)** Two-tailed Spearman's correlation analysis of macrophage
721 apoptosis with (**B**) growth rate or (**C**) granuloma score. Colors indicate lineage, and bars represent
722 medians. Shapes stand for (**A**) independent donors, or (**B-C**) individual strains within the same
723 lineage (LXA in circles, LXB in squares and LXC in triangles). (**A**) Statistical analysis by Friedman test
724 with *post hoc* Dunn's correction. #, $p = 0.058$; **, $p < 0.01$.

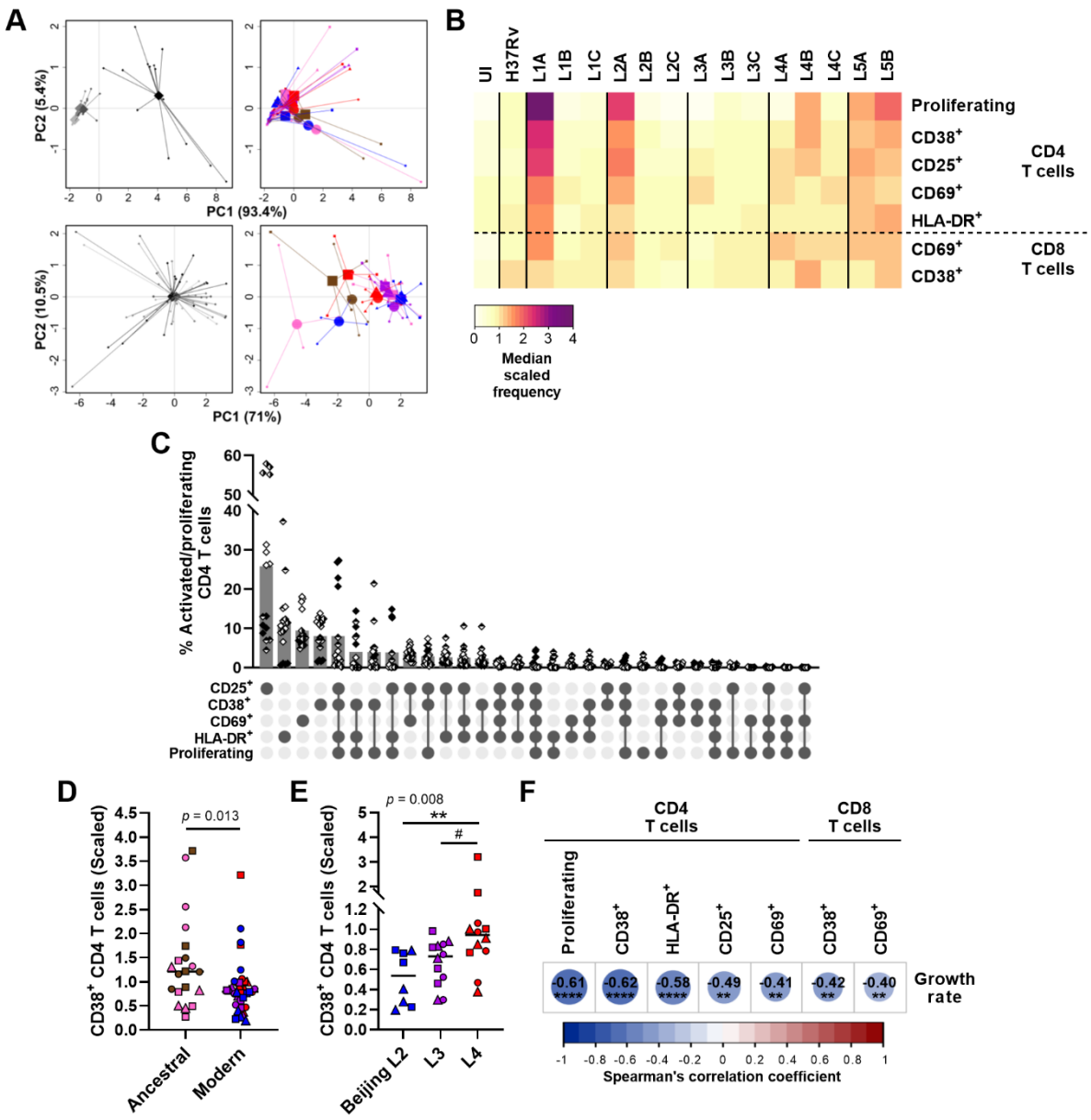

Figure 5. Activation and proliferation of T cells is associated with reduced mycobacterial growth across the MTBC. Percentage of activated (expressing any of the markers) and proliferating (CFSE⁻) T cells on day 6 p.i. was quantified by flow cytometry. **(A)** Principal component (PC) analysis using raw (top panels) or scaled (lower panels) data. Data were grouped by donor (left panels), grey shades represent independent donors; or by MTBC infecting strain (right panels), colors indicate lineage and shapes stand for individual strains within the same lineage (LXA in circles, LXB in squares and LXC in triangles). **(B)** Heatmap representing the median scaled frequencies induced by each MTBC strain. UI, uninfected. **(C)** Marker co-expression on the activated/proliferating CD4 T cells induced by L1A, L2A and L5 strains. Bars represent the mean percentage of cells expressing the indicated marker combination and each filling pattern of the shapes corresponds to an individual donor. **(D-E)** Percentage of CD38⁺ CD4 T cells elicited by (**D**) ancestral or modern lineages, or (**E**) specific modern

737 lineages. Colors and shapes same as in (**A**), and horizontal lines represent medians. Statistical
738 analysis by (**D**) two-tailed Mann-Whitney, or (**E**) Kruskal-Wallis test with post hoc Dunn's correction.
739 **(F)** Heatmap of Spearman's correlation coefficients of activated/proliferating T cell populations with
740 MTBC growth rate (two-tailed, *post hoc* Benjamini-Hochberg corrected). # $p = 0.09$; **, $p < 0.01$;
741 ****, $p < 0.0001$.

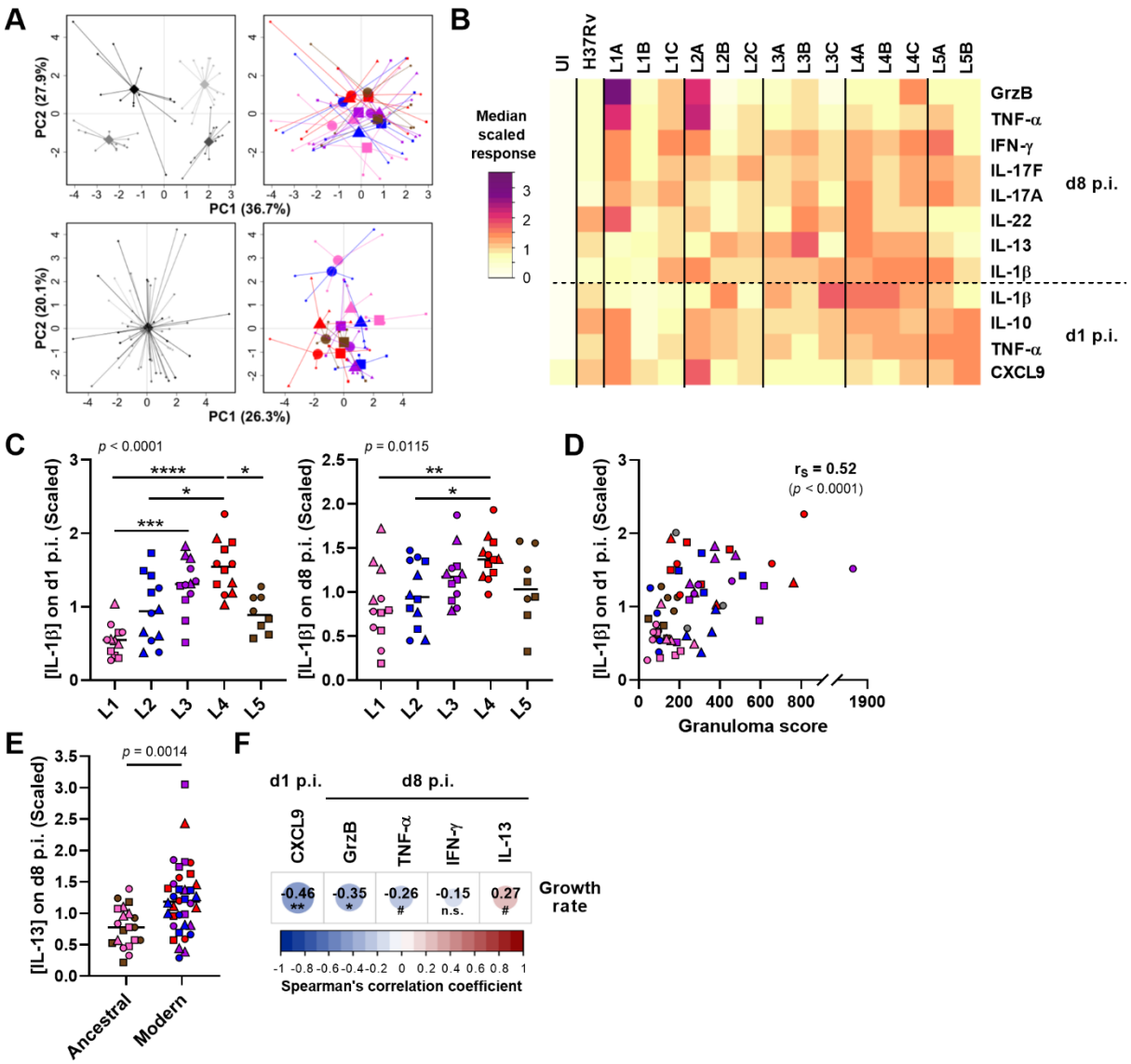

Figure 6. CXCL9, granzyme B and TNF-α secretion is associated with reduced mycobacterial growth across the MTBC. The concentration of soluble mediators in the supernantant of *in vitro* granulomas on days 1 and 8 p.i. was quantified by multiplex bead-based immunoassay. **(A)** Principal component (PC) analysis was performed using raw (top panels) or scaled (lower panels) concentrations. Data were grouped by donor (left panels), grey shades represent independent donors; or by MTBC infecting strain (right panels), colors indicate lineage and shapes stand for individual strains within the same lineage (LXA in circles, LXB in squares and LXC in triangles). **(B)** Heatmap of the median scaled response induced by each MTBC strain. UI, uninfected; GrzB, granzyme B. **(C)** IL-1β response stratified by lineage. **(D)** Two-tailed Spearman's correlation analysis of IL-1β response on day 1 p.i. with granuloma score. **(E)** IL-13 response stratified by ancestral or modern lineages. (**C-E**) Colors and shapes same as in (**A**) and horizontal lines represent medians. Statistical analysis by (**C**) Kruskal-Wallis test, with *post hoc* Dunn's correction, or (**E**) two-tailed Mann-Whitney test. *, $p < 0.05$; **, $p < 0.01$;

755 ***, $p < 0.001$; ****, $p < 0.0001$. (**F**) Heatmap representing Spearman's correlation coefficients with
756 MTBC replication rate (two-tailed, *post hoc* Benjamini-Hochberg corrected). n.s., $p > 0.1$; #, $p = 0.056$;
757 *, $p < 0.05$; **, $p < 0.01$.

758

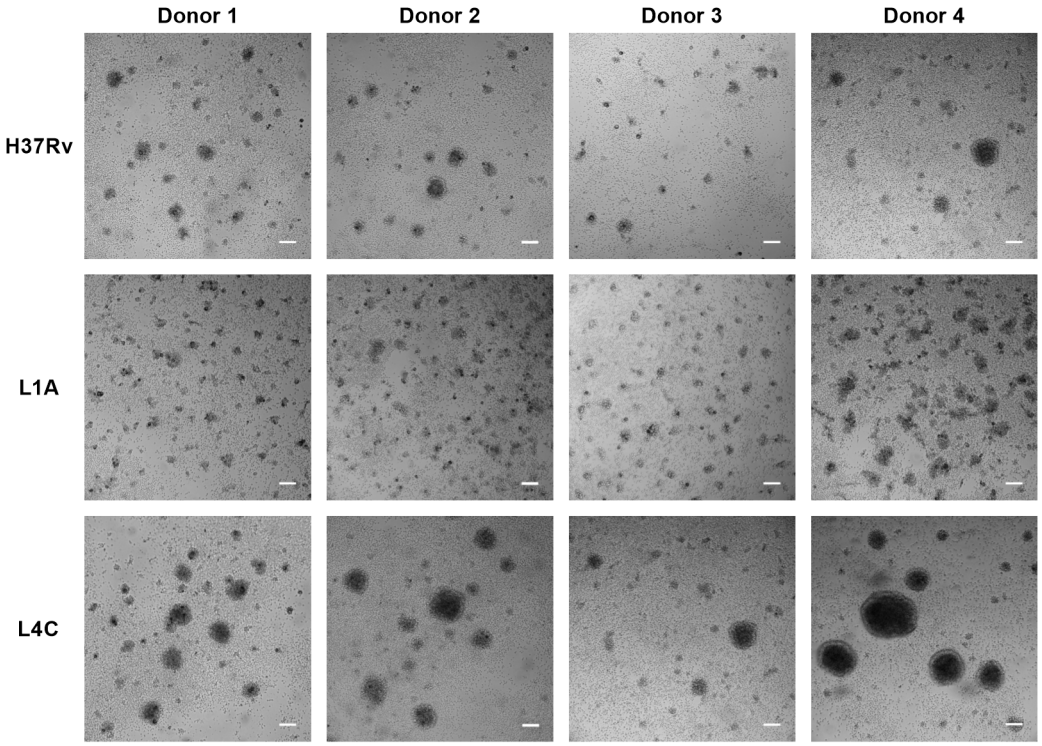

759 **Supplementary figure 1. Granulomatous response variability across MTBC strains is consistent**
760 **across independent donors.** Bright field images of *in vitro* granulomas on day 7 p.i. from MTBC
761 strains representative of the spectrum of granulomatous responses observed. Scale bar = 100 µm.

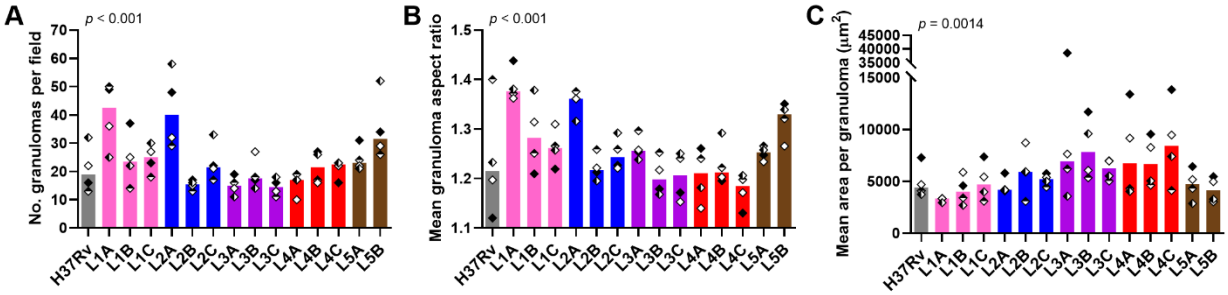

Supplementary figure 2. The number, shape and size of *in vitro* granulomas vary depending on the MTBC infecting strain. (A) Total number (no.) of granulomas, as well as their individual **(B)** aspect ratio and **(C)** area were quantified on a representative bright field for each strain and donor. Colors indicate lineage, shapes correspond to individual donors and bars represent medians. Statistical analysis by Friedman test.

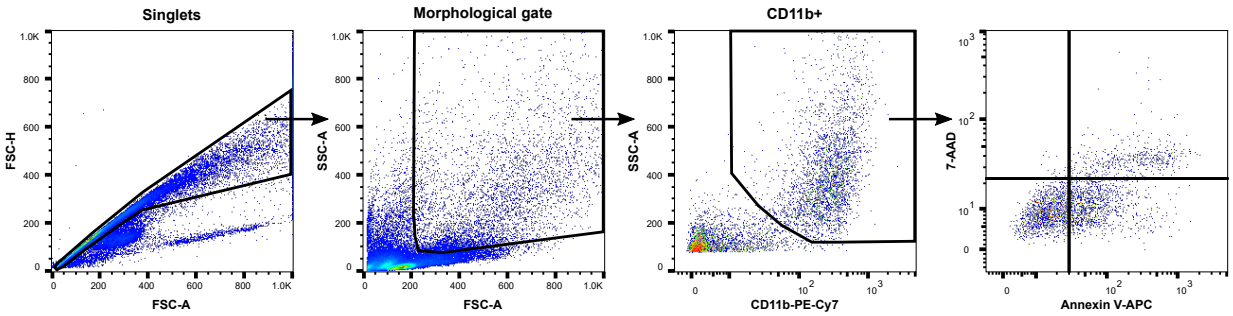

768

769 **Supplementary figure 3. Flow cytometry gating strategy for the quantification of apoptosis**

770 **induction (Annexin V^{+} 7AAD^{-}) in CD11b^{+} macrophages.**

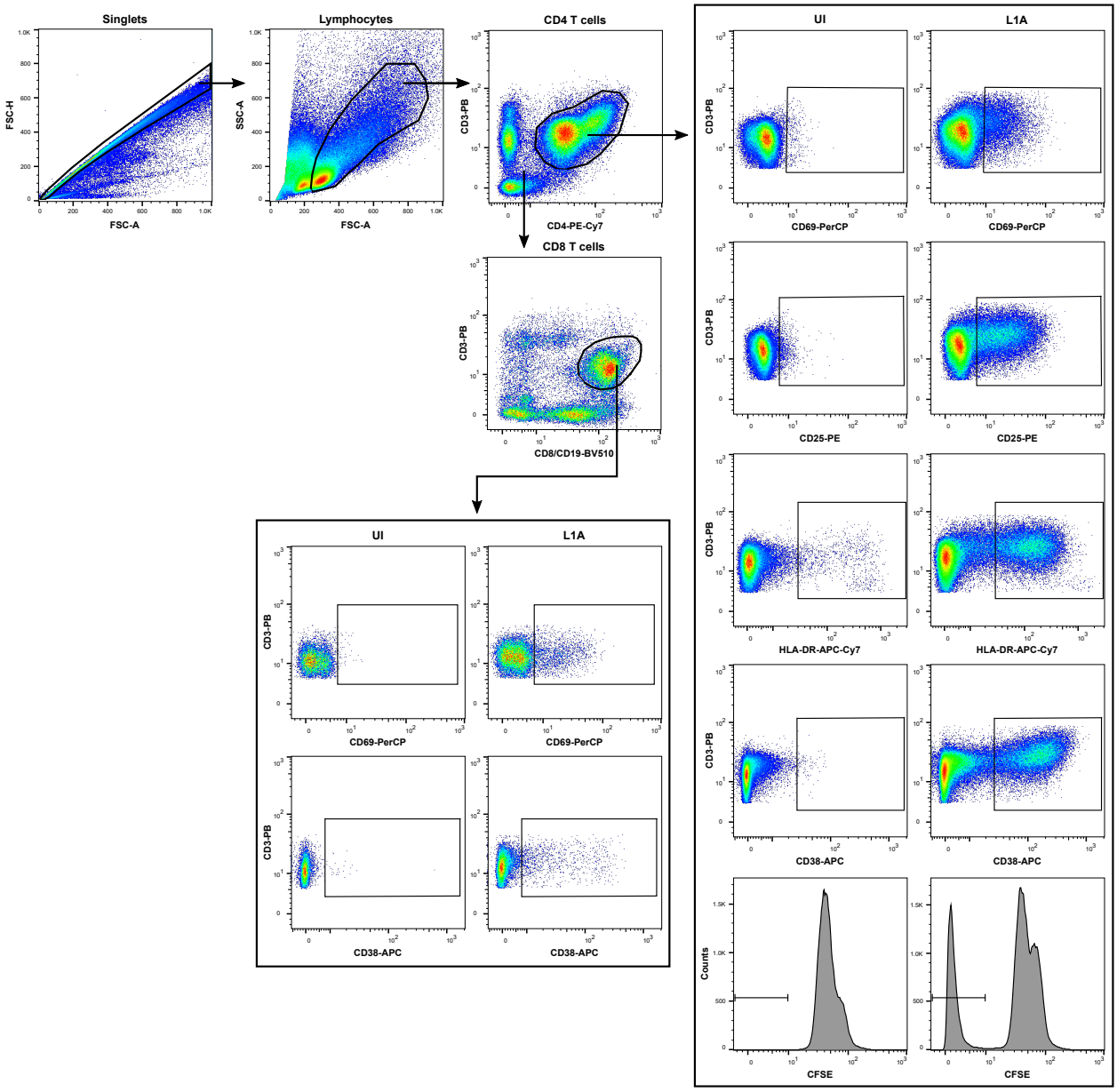

Supplementary figure 4. Flow cytometry gating strategy for the analysis of T cell proliferation and activation. UI, uninfected.

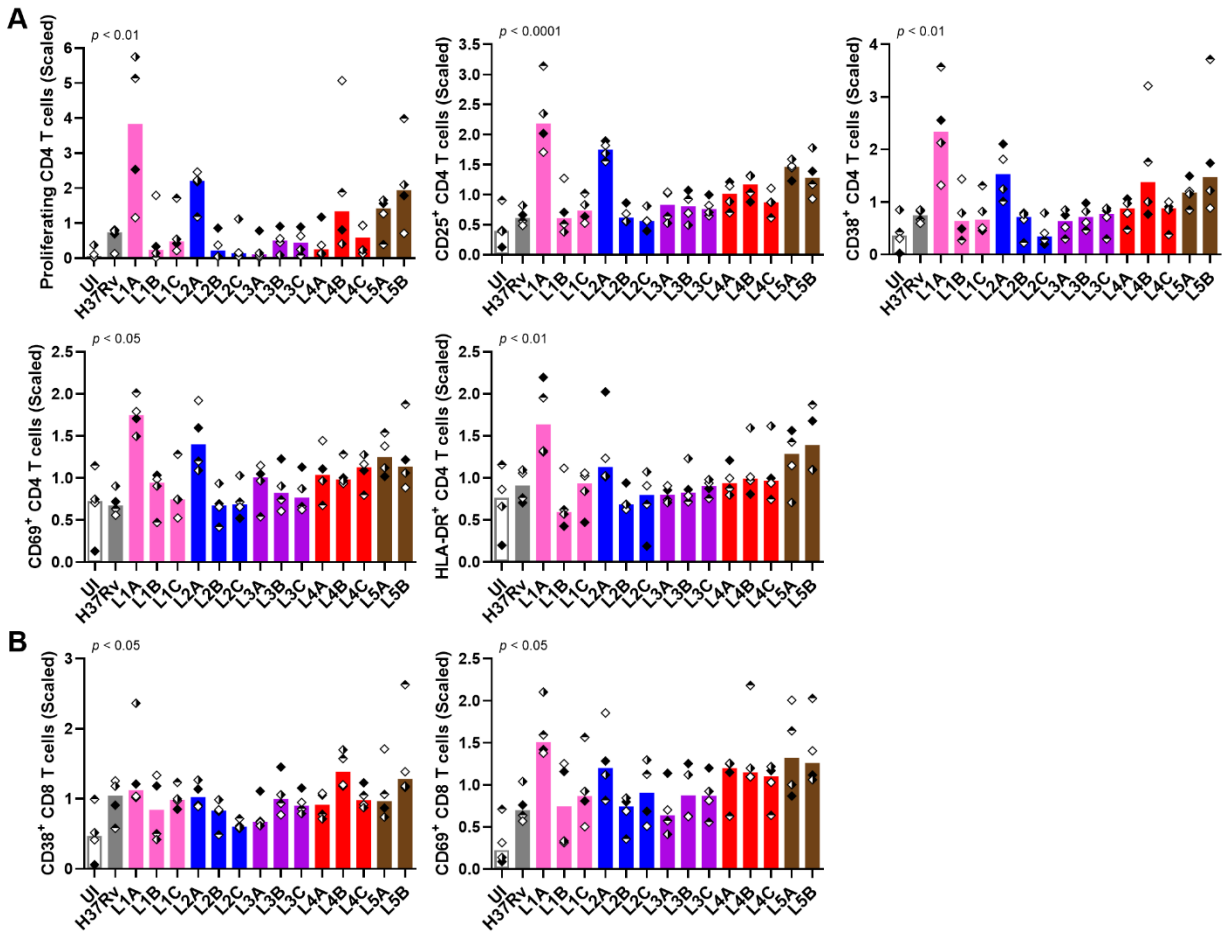

Supplementary figure 5. MTBC strain diversity results in induction of quantitatively distinct T cell responses. Scaled frequencies of **(A)** proliferating and/or activated CD4 and **(B)** CD8 T cells. Colors indicate lineage, each filling of the diamond shapes corresponds to an independent donor and bars represent medians. Statistical analysis by Friedman test. UI, uninfected.

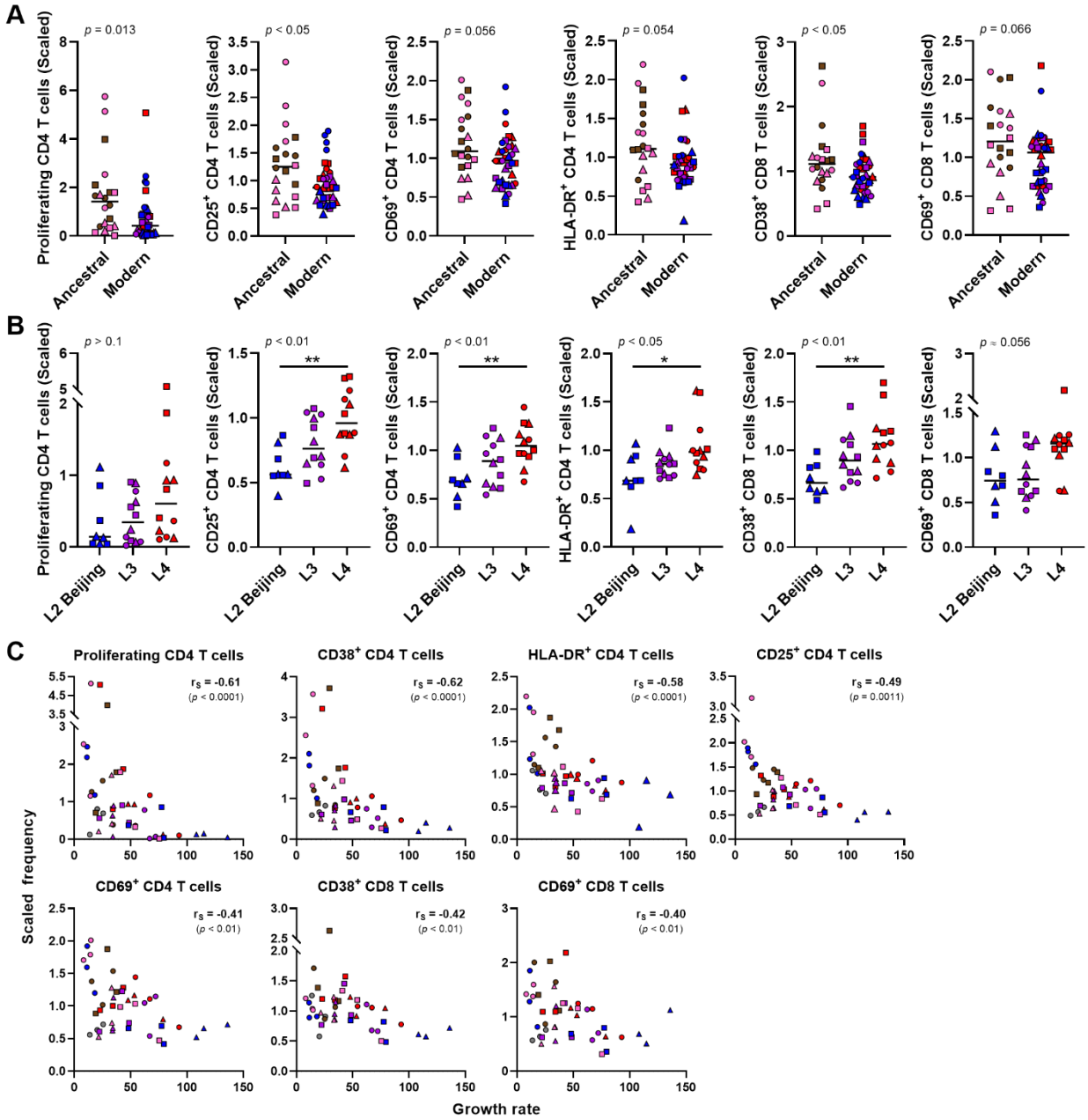

Supplementary figure 6. Induction of T cell activation and proliferation exhibits both lineage- and mycobacterial growth-associated trends. Frequency of each population stratified by **(A)** ancestral or modern lineage, or **(B)** specific modern lineages. Statistical analysis by (**A**) two-tailed Mann-Whitney, or (**B**) Kruskal-Wallis test, with post hoc Dunn's correction. * $p < 0.05$; **, $p < 0.01$. **(C)** Two-tailed Spearman's correlation analyses of the scaled frequencies of the various proliferating/activated T cell populations with MTBC growth rate (*post hoc* Benjamini-Hochberg multiple testing corrected). Colors indicate lineage, shapes stand for individual strains within the same lineage (LXA in circles, LXB in squares and LXC in triangles) and horizontal lines represent medians.

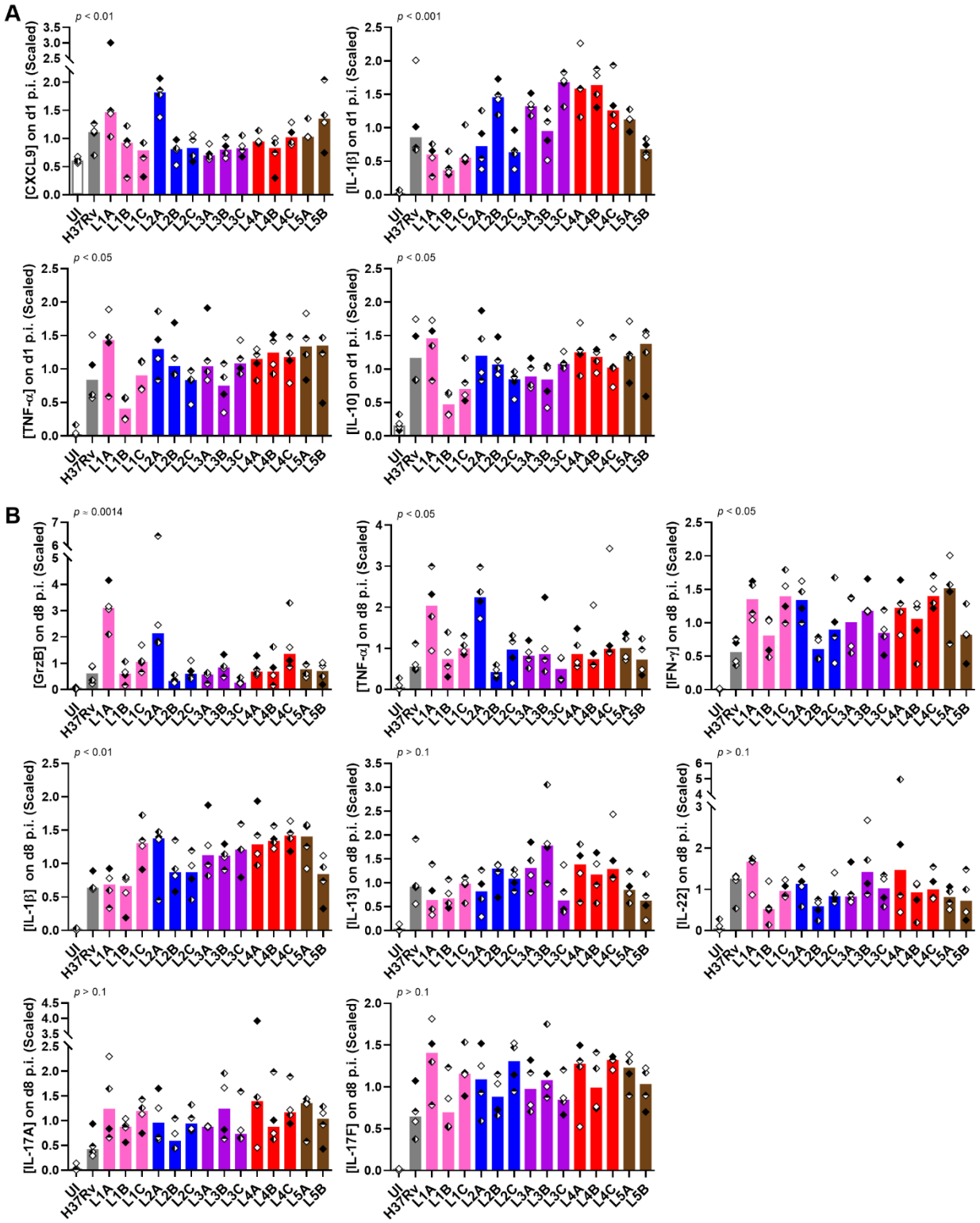

Supplementary figure 7. MTBC diversity results in variable soluble factor immune responses. Scaled concentrations of soluble factors induced by MTBC infection on **(A)** day 1 p.i. or **(B)** day 8 p.i. Colors indicate lineage, each filling of the diamond shapes corresponds to an independent donor and bars represent medians. Statistical analysis by Friedman test. UI, uninfected.

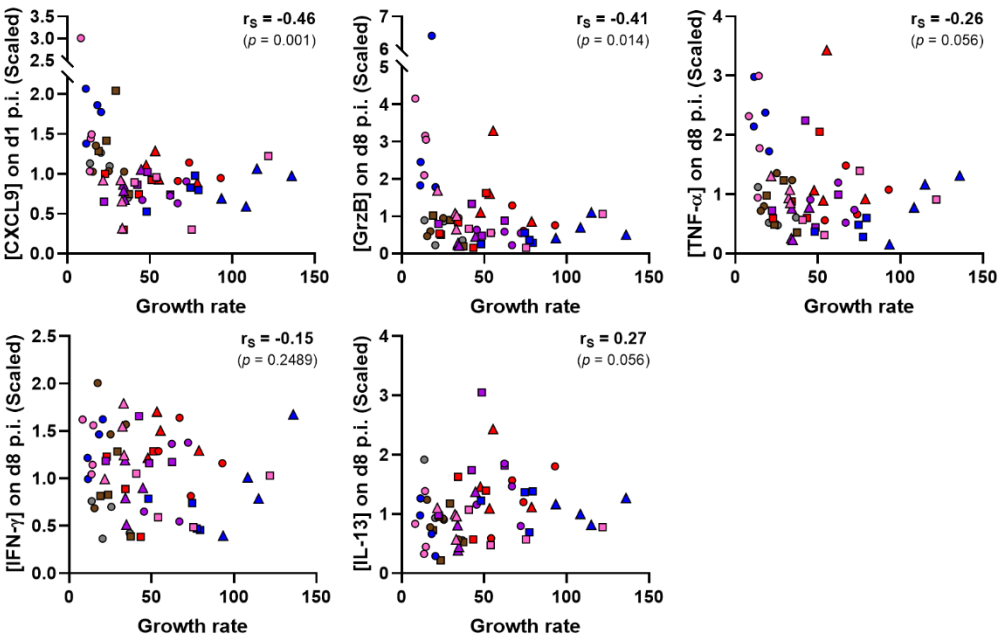

Supplementary figure 8. Several chemokine and cytokine responses associate positively or negatively with MTBC growth rate in *in vitro* granulomas. Two-tailed Spearman's correlation analyses of the indicated soluble factors (scaled concentrations) with MTBC growth rate (*post hoc* Benjamini-Hochberg multiple testing correction). Colors indicate lineage, and shapes stand for individual strains within the same lineage (LXA in circles, LXB in squares and LXC in triangles).